nature communications

Article

https://doi.org/10.1038/s41467-025-63930-0

Mycobacterium tuberculosis-specific T cells restrain anti-cancer drug-induced neutrophilic lung inflammation in tuberculosis

Received: 13 August 2024

Accepted: 30 August 2025

Published online: 06 October 2025

Check for updates

Kee Woong Kwon[1,2,8], Tae Gun Kang[3,4,8], Jii Bum Lee[5], Eunsol Choi[2], Hagyu Kim[2], Min Chul Park[3,4], Sangwon Choi[2], Kyungmin Kim[2], Hyeong Woo Kim[1], Su Jin Jeong[6], Hye Ryun Kim[5], Sung Jae Shin[2,7] ✉ & Sang-Jun Ha[3,4] ✉

Cancers are a risk factor for active tuberculosis (TB), and anti-cancer drugs can independently cause TB progression. To understand the underlying mechanisms, mice infected with *Mycobacterium tuberculosis* (Mtb) were treated with gemcitabine (Gem), cisplatin, or paclitaxel. These treatments delay Mtb-specific T cell responses, increase bacterial loads, and cause hyperinflammation with permissive neutrophils in the lungs. However, depleting Mtb-permissive neutrophils reduce bacterial levels and G-CSF production, thereby attenuating lung immunopathology. Additionally, Mtb-specific T cell responses generated by BCG vaccination inhibit bacterial growth and neutrophil infiltration even after Gem treatment. Gem induces granulocyte-biased generation in the bone marrow via G-CSF signaling, which led to lung neutrophil inflammation. However, pre-existing Mtb-specific T cell responses from BCG vaccination normalizes granulopoiesis by restricting G-CSF production. These findings show the mechanism of anti-cancer drug-induced neutrophilic lung inflammation in TB and highlight the role of Mtb-specific T cell responses in maintaining balanced hematopoiesis against Gem-induced TB immunopathogenesis.

Tuberculosis (TB) remains one of the deadliest infectious diseases, caused by a single infectious agent known as *Mycobacterium tuberculosis* (Mtb). It causes about ten million new cases of active TB and 1.3 million deaths per year. Notably, it is estimated that nearly 25% of the global population harbors a latent Mtb infection. Furthermore, approximately 5–10% of these individuals possess an elevated risk of progressing to an active state during their lifetime[1,2]. This presents a significant challenge for global TB

[1]Department of Microbiology and Convergence of Medical Science, College of Medicine, Gyeongsang National University, Jinju, Republic of Korea. [2]Department of Microbiology, Graduate School of Medical Science, Brain Korea 21 Project, Yonsei University College of Medicine, Seoul, Republic of Korea. [3]Department of Biochemistry, College of Life Science & Biotechnology, Yonsei University, Seoul, Republic of Korea. [4]Brain Korea 21 (BK21) FOUR Program, Yonsei Education & Research Center for Biosystems, Yonsei University, Seoul, Republic of Korea. [5]Division of Medical Oncology, Department of Internal Medicine, Yonsei University College of Medicine, Seoul, Republic of Korea. [6]Department of Internal Medicine, Yonsei University College of Medicine, Seoul, Republic of Korea. [7]Institute for Immunology and Immunological Disease, Yonsei University College of Medicine, Seoul, Republic of Korea. [8]These authors contributed equally: Kee Woong Kwon, Tae Gun Kang. ✉e-mail: sjshin@yuhs.ac; sjha@yonsei.ac.kr

control, considering the large reservoir of individuals at risk of developing active TB.

Despite a limited understanding of TB pathophysiology, the progression to active disease has been linked to several factors, such as age, concurrent conditions like HIV, diabetes mellitus, and nutritional compromise, as well as the use of immunomodulatory drugs[3–6]. This increased risk might be induced by disrupted balance of immune system to prevent infection, progression to primary disease, or reactivation[7]. Specifically, regarding cancer, it has been recognized as a risk factor for active Mtb infection since the 1970s[8], with recommendations for considering latent TB infection (LTBI) screening and treatment as per the guidelines[6,9]. In addition, patients with solid cancers and hematological malignancies have been reported to display a higher risk of TB than the general population and are thought to be immunocompromised due to the disease itself and chemotherapeutic regimens that have adverse effects on the immune system[6,8,10–13]. Moreover, anti-cancer drug, which targets rapidly dividing cancer cells but also has a detrimental impact on other normal cells including those in the bone marrow, resulting in decrease in white blood cell counts and compromised immune function, was reported as independent contributing factor for TB progression in patients with cancer[13]. However, the mechanisms of anti-cancer drug-mediated TB progression in mice and patients with active TB remain unclear.

In line with this, patients with TB were reported to be associated with an increased number of monocytes and neutrophils, and a decreased number of lymphocytes, resulting in a high Monocyte:Lymphocyte (M:L) or Netrophil:Lymphocyte (N:L) ratio compared to those of healthy controls[14–17]. These reports indicated a significant correlation between increased population of neutrophil or monocyte and the progression of active TB[16,18–21]. Additionally, transcriptomic analysis has revealed that increased myeloid cell-related inflammation, secondary to interferon (IFN) responses, is followed by suppressed lymphocytes prior to clinical manifestations in humans and cynomolgus macaques[22,23]. Notably, in human airways, neutrophils are the predominant type of cell infected with Mtb and are found in the inflamed lung lesions of patients with active disease. Furthermore, biomarkers associated with neutrophil activity strongly indicated the TB progression in human[24–28]. In mice, neutrophils have also been reported to contribute to TB progression by being involved in exacerbating disease or acting as a permissive niche favoring bacterial replication[26,27,29–31]. These observations indicate that neutrophil infiltration is a common aspect of TB progression, facilitating both tissue destruction and bacterial replication, irrespective of the underlying causes of susceptibility. However, it remains poorly understood whether chemotherapy for cancer patients, another potential risk factor for TB, also influences neutrophils, a common cellular feature of severe TB, or how it contributes to exacerbating the disease.

Here, in this study, we investigate the underlying mechanisms of anti-cancer drug-driven Mtb susceptibility. Our analysis of the data from cancer patients reveals that treatment with anti-cancer drugs exacerbates TB progression, characterized by neutrophilia and decreased infiltration of lymphocytes. To further investigate these mechanisms, mice were initially infected with the Mtb Beijing clinical strain K, followed by administration of the anti-cancer drug such as gemcitabine (Gem), cisplatin (CP), or paclitaxel (PTX). Mice infected with Mtb and treated with anti-cancer drug exhibit significant increases in bacterial loads and hyperinflammation in the lungs, along with a significant decrease of the Mtb-specific T cell response, compared to those infected only with Mtb. The exacerbation of disease driven by Gem treatment is mitigated by antibody-mediated depletion of neutrophils. Interestingly, a predominance of Mtb-specific T cells induced by BCG immunization confers resistance against the effects of Gem in Mtb-infected mice, leading to ameliorated neutrophil-mediated pulmonary inflammation and controlled bacterial growth. In a mechanistic view, Gem treatment induces granulocyte-biased generation in the bone marrow of Mtb-infected mice by G-CSF downstream signaling, whereas pre-existing Mtb-specific T cell response normalize hematopoiesis resulting in diminished neutrophilic lung inflammation. Overall, our study demonstrates that anti-cancer drug treatment during TB promotes increased bacterial growth and pulmonary immunopathology, suggesting an underlying mechanism whereby Gem exacerbates TB progression by favoring granulopoiesis.

Results

Treatment of anti-cancer drugs aggravates TB progression in cancer-diagnosed patients

To examine the association between anti-cancer drug treatment and TB progression in cancer patients, we collected data from patients who tested positive for Mtb at Severance Hospital between January 2005 and July 2019 (Supplementary Fig. 1). According to our criteria, 7 of the 16 selected patients exhibited neutrophilia accompanied by decreased lymphocytes following treatment with anti-cancer drugs (Fig. 1A), while 9 patients displayed no significant changes in the number of neutrophils and lymphocytes (Supplementary Fig. 2A, B). Additionally, a higher proportion of patients who developed neutrophilia had a tendency to present strong AFB smear positivity (AFB 3+ or 4+, 6/7 patients) compared to those without neutrophilia (4/9 patients) (Supplementary Fig. 3A, B). Here, we describe 3 patients diagnosed with both stage IV cancer and pulmonary TB, who experienced increased neutrophil counts and aggravated TB during treatment. Case (1): a 77-year-old male, diagnosed with stage IV non-small cell lung cancer (NSCLC), initially received 3 cycles of Gem and CP (Fig. 1B). Follow-up computed tomography (CT) revealed disease progression alongside active pulmonary TB. The patient's sputum acid-fast bacilli (AFB) smear and culture were positive for Mtb. Despite anti-TB treatment, a follow-up chest CT, conducted 1 month later, showed worsening of the pulmonary TB. The sputum AFB smear and culture, which previously maintained a negative conversion post anti-TB medication, tested positive again. His neutrophil count, initially around 6000 mm^3, increased to 16,000 mm^3 and remained above 10,000 mm^3, even several weeks after the anti-TB treatment. Case (2): a 56-year-old male was diagnosed with both stage IV advanced gastric cancer (AGC) and pulmonary TB. An X-ray indicated fibrostreaky densities in the left upper lung, and his sputum AFB smear and culture tested positive for Mtb (Fig. 1C). The patient was treated with anti-TB medication for 2 weeks and maintained negative sputum AFB and culture results. The patient's tumor burden was localized to the stomach with no evidence of lung metastasis. The patient subsequently underwent palliative gastrectomy and received treatment with PTX and CP. However, after 6 weeks of chemotherapy, a chest X-ray showed aggravation and reactivation of pulmonary TB. The sputum AFB smear and culture tested positive for Mtb once again. The patient's neutrophil count, which decreased from 8000 to 2000 mm^3 after the TB treatment, steadily increased during the cancer treatment and peaked at 6000 mm^3. Case (3): a 73-year-old male was diagnosed with stage IV AGC with carcinomatosis and was treated with PTX + CP chemotherapy. After three cycles, the patient developed worsening pulmonary symptoms including dyspnea, cough, and sputum production. Chest X-ray revealed increasing haziness in the left lung. Sputum AFB smear and culture tested positive for Mtb (Fig. 1D). The patient was initiated on anti-TB therapy, leading to clinical improvement and gradual resolution of pulmonary infiltrates. After 2 months of treatment, sputum AFB smear and culture converted to negative. At the time of TB diagnosis, the patient's neutrophil count had increased from 3000 to 6000/mm^3 during chemotherapy, peaking at 8000/mm^3, while lymphocyte levels concurrently declined. These findings suggest that chemotherapy-induced neutrophilia may have contributed to TB reactivation or exacerbation.

https://doi.org/10.1038/s41467-025-63930-0

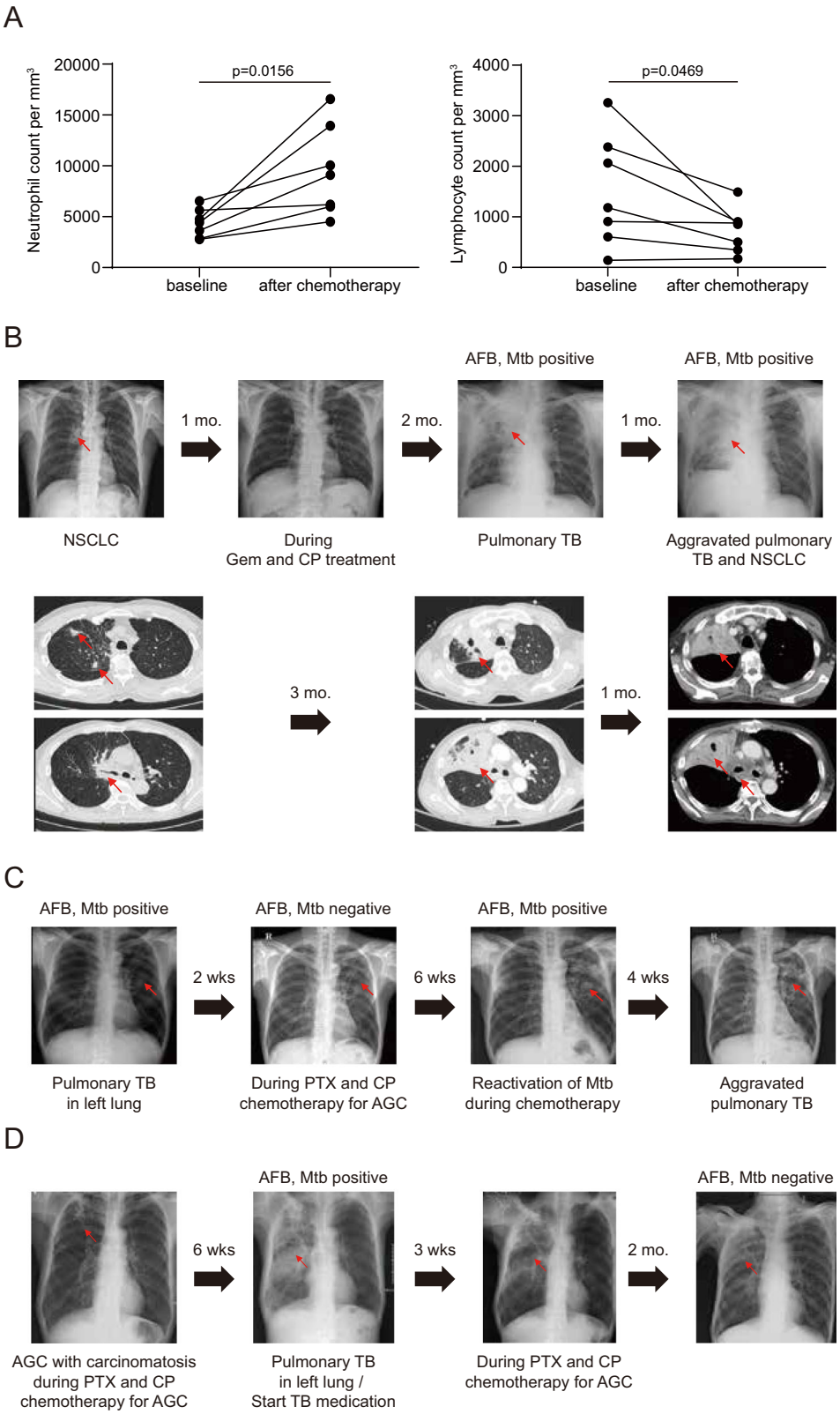

Fig. 1 | Aggravated pulmonary TB in cancer-diagnosed patients after treatment of anti-cancer drugs. A The number of neutrophils and lymphocytes from blood of cancer-diagnosed patients who developed to active TB after treatment of anti-cancer drug ($n = 7$). Two-tailed Wilcoxon matched pairs test was used to compare baseline and after treatment. *$p < 0.05$. **B** Description of non-small cell lung cancer (NSCLC) patient with pulmonary TB. **C**, **D** Description of advanced gastric cancer (AGC) patients with pulmonary TB. Source data are provided as a Source Data file.

https://doi.org/10.1038/s41467-025-63930-0

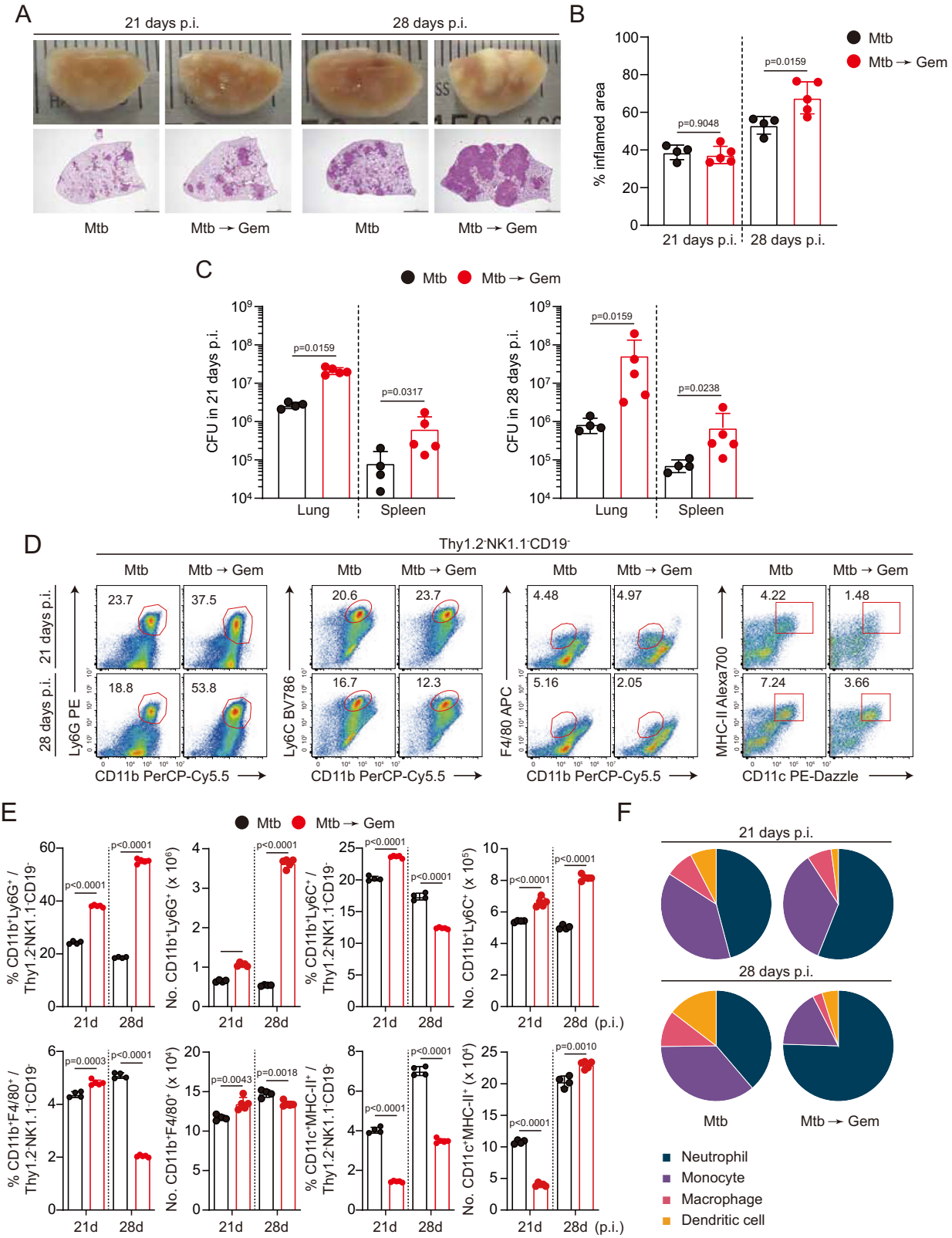

Anti-cancer drugs aggravate TB progression with neutrophilia in mice

To investigate the effects of anti-cancer drugs on TB progression in vivo, we first established an experimental mouse model. Mice were aerogenically infected with Mtb K and subsequently administered the anti-cancer drugs such as Gem, CP, or PTX via the intraperitoneal route, 3 times at 2-day intervals, starting from 14 days post-Mtb infection. The mice were then sacrificed at 21 and 28 days post-Mtb infection. Gem-treated mice displayed exacerbated pulmonary pathology with necrotic granulomatous lesions at 28 days post-Mtb infection compared to the mice subjected to Mtb K infection alone (Fig. 2A, B). While there was no obvious exacerbated lung pathology at 21 days post-Mtb infection in Gem-treated mice, the bacterial burdens in both the lungs and spleen of Gem-treated mice were significantly

Fig. 2 | Severe TB immunopathology in Mtb-infected mice followed by gemcitabine (Gem) treatment. A C57BL/6J mice were infected with Mtb K strain alone or Mtb K followed by treatment with anti-cancer drug at 13, 15, and 17 days post Mtb infection. At 21 and 28 days post Mtb infection, mice were sacrificed ($n = 4, 5$). Gross pathology or H&E staining of lungs in each group. (10×, scale bars = 2.0 mm). **B** The data represent the percentages of the superior lobe of the right lung showing inflammation ($n = 4, 5$). The graph shows the mean ± SD. Data were analyzed by two-tailed Mann–Whitney rank test. **C** Bacterial loads in the organs of each group ($n = 4, 5$). The graph shows the mean ± SD. Two-tailed Mann–Whitney rank tests were used to compare groups. n.s. not significant and $^{*}p < 0.05$. **D**, **E** The frequency and number of $CD11b^{+}Ly6G^{+}$, $CD11b^{+}Ly6C^{+}$, $CD11b^{+}F4/80^{+}$, and $CD11c^{+}MHC\text{-}II^{+}$ cells. The numbers in the plot indicate the percentage of cells ($n = 4, 5$). The graph shows the mean ± SD. Data were analyzed by two-tailed unpaired *t*-test. n.s. not significant, $^{**}p < 0.01$, $^{***}p < 0.001$, and $^{****}p < 0.0001$ between group. **F** The compositions of lung immune cell populations in Mtb-infected mice are presented in pie charts. **A**–**F** The data are representative of at least two independent experiments. Source data are provided as a Source Data file.

increased at both 21 and 28 days post-Mtb infection compared to those in mice infected with Mtb K alone (Fig. 2C). Additionally, disease severity was dependent on the infection dose; a high-dose infection of Mtb (~360 CFU) induced an earlier occurrence of death in mice treated with Gem but a low-dose infection of Mtb (~ 150 CFU) did not (Supplementary Fig. 4). For low-dose Mtb infection, Gem-treated mice also exhibited TB progression at 28 and 70 days post-Mtb infection, characterized by exacerbated pulmonary pathology and increased bacterial burdens in the lungs and spleen (Supplementary Fig. 5A–C). Abundant Mtb was detected in the lungs by AFB and rhodamine staining (Supplementary Fig. 5D, E).

As observed in Gem-treated mice, treatment with CP or PTX also aggravated TB disease progression, evidenced by exacerbated lung inflammation and increased bacterial loads in the lungs and spleen compared to Mtb K-infected mice (Supplementary Fig. 6A–C). Given that Gem was the most widely used among selected patients (12 out of 16) (Supplementary Fig. 1) and its effect on Mtb-infected mice was most pronounced in terms of lung inflammation and bacterial loads compared to either PTX or CP (Supplementary Figs. 5 and 6), we continued to use Gem in subsequent studies. Next, we characterized the immune cells in the lungs by their cell surface phenotypes to identify the populations mediating severe TB immunopathology following Gem treatment during TB infection (Supplementary Fig. 7). Consistent with previous studies that associate neutrophilic inflammation with disease severity in TB[29,32,33], we observed a significant increase in the frequency and number of $CD11b^{+}Ly6G^{+}$ neutrophils in Mtb-infected mice following Gem treatment at 21 days post-infection, compared to those with Mtb infection alone. This trend of increase in neutrophil populations was also apparent 28 days post-infection (Fig. 2D, E). In addition, an increased number of $CD11b^{+}Ly6C^{+}$ monocytes was observed at 21 and 28 days post-Mtb infection, while a decreasing trend in the number of $CD11c^{+}MHC\text{-}II^{+}$ dendritic cells, and $CD11b^{+}F4/80^{+}$ macrophages was significant at 21 and 28 days post-Mtb infection, respectively, compared to those of Mtb-infected alone (Fig. 2D, E). Consequently, a neutrophil-dominant environment in the lung was established upon Gem treatment during TB (Fig. 2F). In an independent experimental setting with low-dose Mtb infection, similar changes in pulmonary myeloid cell population were also observed (Supplementary Fig. 8A, B). Given that myelosuppression is the most common side effect of chemotherapeutic drugs[34], we then analyzed infiltrated immune cells in the lungs of naïve mice following Gem treatment. Although neutrophils and monocytes in the lungs were reduced starting from 1 day post Gem treatment, the decreased frequencies of these cell populations were all restored after 7 days of Gem treatment, which reflects the time point of 21 days post Mtb infection (Supplementary Fig. 9), suggesting that the reconstitution of cell populations upon Gem treatment may affect the proportion of immune cells in the lung during TB. In summary, these data suggest that treatment of anti-cancer drugs increases the disease severity of Mtb-infected mice, establishing a neutrophil-dominant environment.

Gem treatment in Mtb-infected mice delays pulmonary Th1 response

Next, we analyzed Mtb-specific T cells, which are well-documented for mediating host resistance against Mtb infection[35]. We determined the frequency and number of $ESAT6_{4\text{-}17}$:I-A(b)- or $Ag85B_{280\text{-}294}$:I-A(b)-specific $CD4^{+}$ T cells by tetramer staining. Notably, both ESAT6- and Ag85B-specific $CD4^{+}$ T cells were barely detected in Gem-treated group, in contrast to the Mtb-only infected group at 21 days post-Mtb infection. Then, ESAT-6-specific $CD4^{+}$ T cells were observed at 28 days post-Mtb infection, although their frequency and number were reduced compared to the Mtb-only infected group. Similarly, Ag85B-specific $CD4^{+}$ T cells exhibited increased frequency and number at 28 days post-Mtb infection, which were even higher than the Mtb-only infected group (Fig. 3A, B). Ex vivo stimulation of an ESAT-6 peptide pool, covering all peptides derived from ESAT-6 protein, or Ag85B protein indicated that ESAT-6- or Ag85B-specific $CD4^{+}$ T cells from the Mtb-infected group produced IFN-γ and TNF at substantial levels, whereas the functions of these cells in the Gem-treated group dramatically decreased at 21 days post-Mtb infection (Fig. 3C, D). At 28 days post-Mtb infection, restored frequencies and numbers of both Mtb-specific $CD4^{+}$ T cells producing IFN-γ and TNF were detected, exhibiting similar trends to tetramer staining in Mtb-infected mice following Gem treatment compared to Mtb only-infected mice (Fig. 3C, E). In an independent experimental setting with low-dose Mtb infection, we also observed that significantly curtailed frequency of ESAT-6-specific $CD4^{+}$ T cell responses producing IFN-γ and TNF at 21 days post-Mtb infection in the Gem-treated group was restored at 28 days post-Mtb infection to levels comparable to the Mtb only-infected group, including $TB10.4_{4\text{-}12}$-specific $CD8^{+}$ T cells producing IFN-γ and TNF (Supplementary Fig. 10A, B). Taken together, these data show that the number and response of Mtb-specific T cells are significantly delayed in Gem-treated mice.

Depletion of $Ly6G^{+}$ neutrophils reduces bacterial burden and ameliorates lung immunopathology

Together with neutrophilia observed in our model (Fig. 2D–F), we further investigated whether the increased neutrophils population ($CD11b^{+}Ly6G^{+}$) contributes to disease exacerbation by providing a preferential replication site for Mtb. As neutrophils act as a niche for Mtb by remaining proportional to the number of bacterial burdens in the lung[27], we isolated $CD11b^{+}Ly6G^{+}$ neutrophils from the lungs of either only Mtb-infected mice or Mtb-infected mice followed by Gem treatment and measured bacterial burdens in these cells at 28 days post Mtb infection. We found that $CD11b^{+}Ly6G^{+}$ cells from Gem-treated mice harbored higher bacterial loads than those from mice infected only with Mtb (Fig. 4A). Subsequently, we specifically depleted $Ly6G^{+}$ cells by using an anti-Ly6G (1A8) antibody (Fig. 4B). Notably, the anti-Ly6G antibody depleted neutrophils in the lungs of Gem-treated mice (Fig. 4C) and the depletion of $Ly6G^{+}$ cells significantly reduced lung inflammation at the level of the Mtb-infected alone group (Fig. 4D, E). Although bacterial loads were not decreased to the level of the Mtb-infected alone group, a significant bacterial reduction was observed in Gem-treated group followed by depletion of $Ly6G^{+}$ cells compared to Gem-treated isotype control group (Fig. 4F). Furthermore, administration of anti-Ly6G antibody significantly decreased the levels of inflammatory cytokines in lung lysates, including IL-1β, TNF, MCP-1, IL-17, and IL-10 (Fig. 4G). The restoration of IFN-γ in lung lysates was more pronounced upon Ly6G depletion than Gem-treated isotype control group, showing no

https://doi.org/10.1038/s41467-025-63930-0

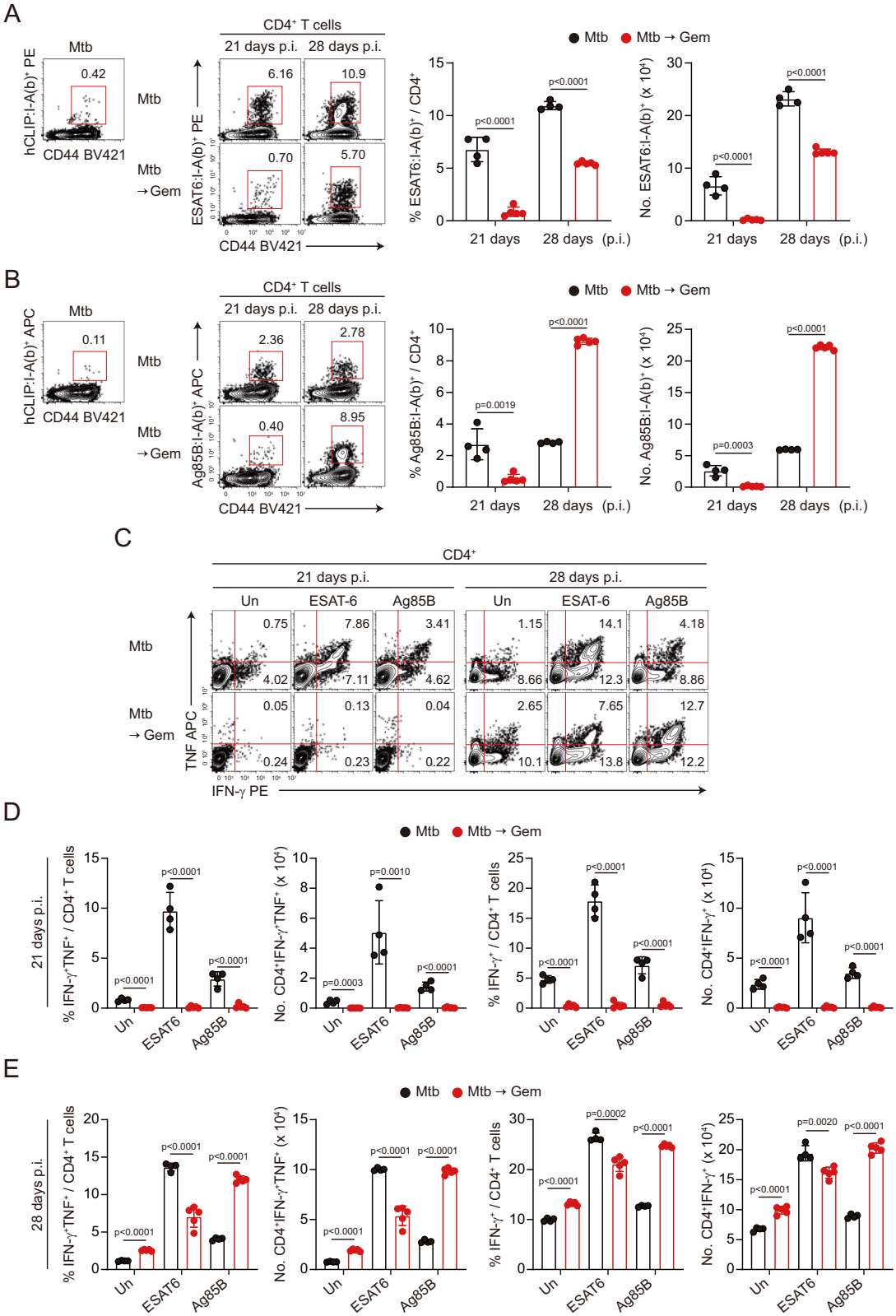

Fig. 3 | Reduced Th1 responses in Mtb-infected mice followed by gemcitabine (Gem) treatment. A, B The frequencies and numbers of $ESAT6_{4\text{-}17}$:I-A(b)- or $Ag85B_{280\text{-}294}$:I-A(b)-specific $CD4^+$ T cells identified by tetramer staining were analyzed by flow cytometry. The numbers in the plots indicate the percentage of tetramer-positive cells among $CD4^+$ T cells ($n = 4, 5$). The graph shows the mean ± SD. Data were analyzed by two-tailed unpaired *t*-test. **C**–**E** The frequencies and numbers of IFN-γ- and TNF-producing $CD4^+$ T cells were analyzed by flow cytometry ($n = 4, 5$). The graph shows the mean ± SD. Data were analyzed by two-tailed unpaired *t*-test. $^{**}p < 0.01$, $^{***}p < 0.001$, and $^{****}p < 0.0001$ between group. **A**–**E** The data are representative of at least two independent experiments. Source data are provided as a Source Data file.

https://doi.org/10.1038/s41467-025-63930-0

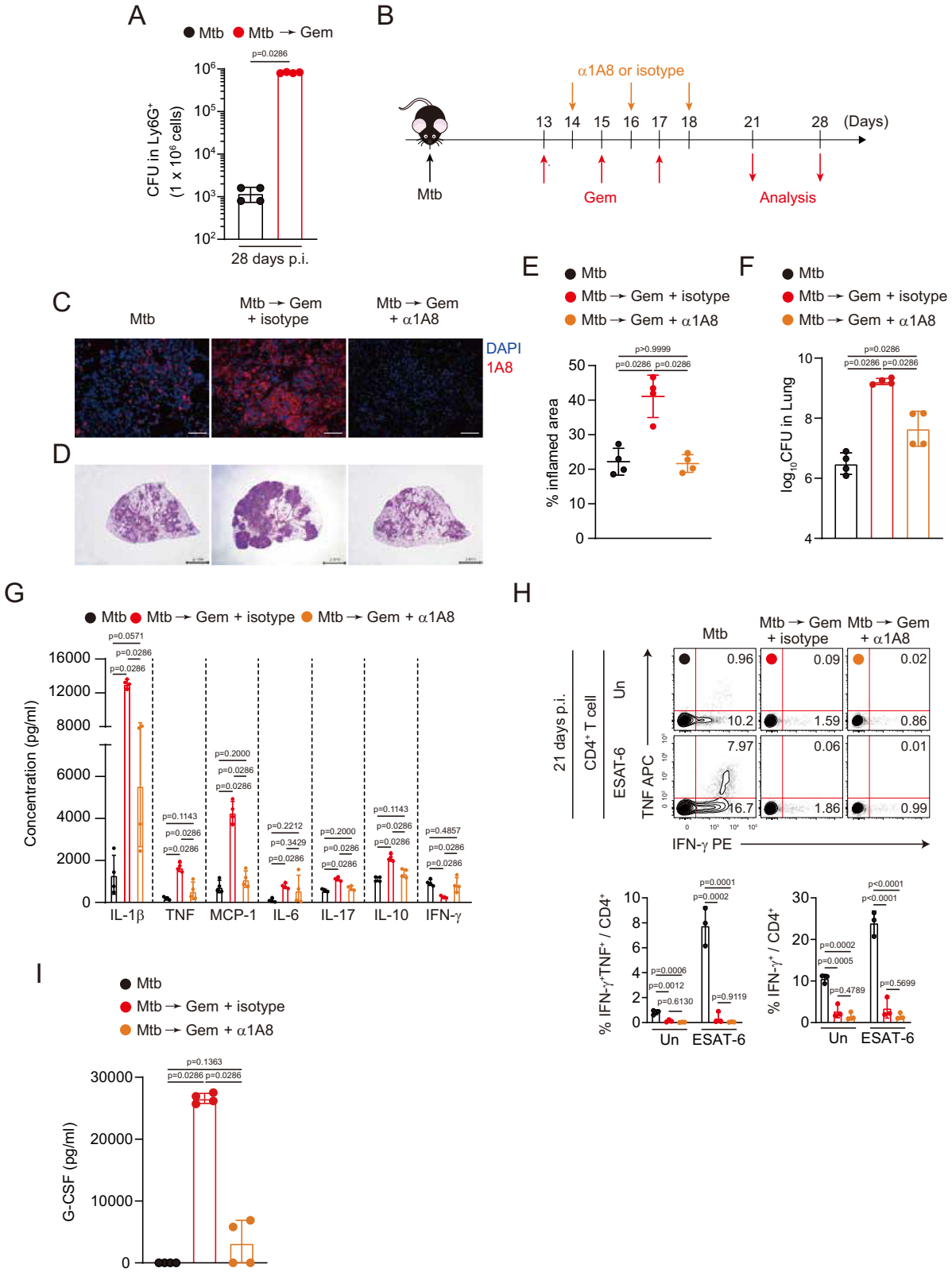

significant differences in cytokine production compared to the Mtb only-infected group at 28 days post-Mtb infection (Fig. 4G). However, Mtb-specific T cell responses were still not detectable at 21 days post-Mtb infection upon Ly6G depletion in Gem-treated mice (Fig. 4H), indicating the delayed pulmonary Th1 responses shown in Fig. 3D, E. Additionally, increased production of G-CSF, which has been reported to be associated with generation of granulocytes[36–38], was also dramatically reduced in serum of Gem-treated mice upon depletion of Ly6G$^+$ cell population (Fig. 4I).

Considering that neutrophils in Gem-treated group displayed increased expression of arginase-1 (ARG1) at 21 and 28 days post-Mtb infection, and Nos2 at 28 days post-infection (Supplementary Fig. 11A), we subsequently investigated whether the neutrophils population acts as myeloid-derived suppressor cells (MDSCs) to suppress Mtb-specific

Fig. 4 | Reduced bacterial loads and lung inflammation without restoration of Mtb-specific T cell responses in gemcitabine (Gem)-treated mice upon depletion of Ly6G$^+$ cells. A 28 days post Mtb infection, equal numbers of isolated CD11b$^+$Ly6G$^+$ cells from Mtb-infected mice (~350 CFU) and Mtb-infected mice treated with Gem were lysed with 0.05% Triton X-100, and the lysates were plated onto 7H10 agar to enumerate the bacteria ($n = 4$). The graph shows the mean ± SD. Data were analyzed by two-tailed Mann–Whitney rank test. **B** At 14, 16, and 18 days post Mtb infection, a monoclonal anti-Ly6G antibody (α1A8) or isotype control was administered i.p. into Gem treated mice. Then, mice were sacrificed at 21 and 28 days post Mtb infection. **C**, **D** Immunofluorescence and H&E staining of the lungs at 28 days post Mtb infection (10×, scale bars = 2.0 mm; 400×, scale bars, 50 μm). **E** The percentages of inflamed area in the lungs at 28 days post Mtb infection ($n = 4$). The graph shows the mean ± SD. Data were analyzed by two-tailed Mann–Whitney rank test. **F** CFUs in the lungs at 28 days post Mtb infection, determined by counting the viable bacteria ($n = 4$). The graph shows the mean ± SD. Data were analyzed by two-tailed Mann–Whitney rank test. **G** The levels of cytokines in lung homogenates obtained from 28 days post Mtb infection were analyzed by ELISA ($n = 4$). The graph shows the mean ± SD. Two-tailed Mann–Whitney rank tests were used to compare groups. n.s. not significant, $^*p < 0.05$. **H** The frequencies of IFN-γ- and TNF-producing CD4$^+$ T cells were analyzed by flow cytometry. The graph shows the mean ± SD from pooled samples ($n = 3$) from each group ($n = 4$). Data were analyzed by one-way ANOVA with post hoc Tukey test. n.s. not significant, $^{**}p < 0.01$, $^{***}p < 0.001$, and $^{****}p < 0.0001$ between group. **I** The level of G-CSF in serum at 28 days post Mtb infection were analyzed by ELISA ($n = 4$). The graph shows the mean ± SD. Two-tailed Mann–Whitney rank tests were used to compare groups. n.s. not significant, $^*p < 0.05$. **A**, **G**–**I** The data are representative of a single experiment or **C**–**F** at least two independent experiments. Source data are provided as a Source Data file.

T cell response[39]. We performed T cell suppression assays using isolated CD11b$^+$Ly6G$^+$ cells from the lungs of only Mtb-infected mice and Mtb-infected mice followed by Gem treatment (Supplementary Fig. 11B, C), resulting in no significant difference of suppression capacity among all groups (Supplementary Fig. 11D). As a control cells, CD11b$^+$Ly6G$^+$ cells isolated from established lung tumor after intravenous injection of lung adenocarcinoma cell line TC-1 significantly inhibited the proliferation of T cells, consistent with a previous finding[40] (Supplementary Fig. 11E). Collectively, our data suggest that increased CD11b$^+$Ly6G$^+$ neutrophils upon Gem treatment are the main culprits that exacerbate TB progression.

Gem treatment post-Mtb infection affects the priming and clonal expansion of Mtb-specific T cells

As shown in Fig. 3, Gem treatment post-Mtb infection led to delayed Mtb-specific CD4$^+$ T cell responses. To further investigate the effect of Gem on Mtb-specific T cell response, we purified CD4$^+$ T cells from P25-Tg mice (Thy1.1$^+$) expressing a TCR specific for the Mtb antigen Ag85B[41], and adoptively transferred them to naïve mice (Thy1.2$^+$). This approach was taken because, at the time of Gem treatment, there are very few Mtb-specific T cells present in the lung[42]. At 1 day after adoptive transfer, mice were infected with Mtb and subsequently administered with Gem 3 times at 2-day intervals, starting 13 days post-Mtb infection (Fig. 5A). As expected, disease exacerbation evidenced by increased bacterial loads, pulmonary inflammation, and neutrophils was induced in Gem-treated mice compared to Mtb-infected only mice at 21 days post Mtb infection (Fig. 5B and Supplementary Fig. 12A, B), indicating that single Mtb epitope-specific naïve CD4$^+$ T cell population is not enough to regulate the increase of bacterial burden and immunopathology after Gem treatment of Mtb-infected mice. Interestingly, unlike endogenous CD4$^+$ T cells in the recipient mice (Fig. 5C), the frequency and number of adoptively transferred P25 cells were similar in the lung of between Mtb-infected alone and Mtb-infected mice followed by Gem treatment (Fig. 5D). Given that major pulmonary influx of P25 occurred between 14 days and 21 days post Mtb infection[35], we found that P25 cells in the draining lymph nodes (dLNs) displayed high proliferating capacity with an increased expression of Ki67 at 14 days post Mtb infection (Supplementary Fig. 13A, B). These data indicate that highly proliferating P25 cells in the dLNs are not affected by anti-cancer drug treatment and thus, can be subsequently infiltrated into the lung. Additionally, although those of Ki67$^+$ cells and CD44$^+$ cells among endogenous CD4$^+$ T cells in the recipient mice were dramatically reduced after Gem treatment (Fig. 5E), the frequencies of Ki67$^+$ cells and CD44$^+$ cells were preserved only in P25 T cells in the lung against Gem treatment at 21 days post Mtb infection (Fig. 5F). Furthermore, we analyzed the function of P25 T cells after ex vivo stimulation with Ag85B peptides using lung single cells isolated from each group. At 21 days post Mtb infection, P25 T cells in the lung were not affected by Gem treatment, as they produced IFN-γ and TNF upon stimulation with Ag85B peptides at levels comparable to those from Mtb-infected only group (Fig. 5G). Collectively, these findings suggest that Gem treatment after Mtb infection suppresses the priming and clonal expansion of endogenous Mtb-specific T cells, which exist at low frequency, leading to delayed Th1 responses. However, their migration to the lungs might remain unaffected by the treatment in the presence of Mtb-specific T cells at high frequency prior to Gem treatment.

BCG vaccination restrains Gem-induced exacerbation of TB pathogenesis

Based on this observation, we examined whether established Th1 responses could mediate resistance against Gem treatment during TB. Thus, using a time-dependent Gem treatment model, mice treated with Gem at 14 days after Mtb infection consistently displayed exacerbated immunopathology along with increased bacterial burdens (Supplementary Fig. 14A–C). However, at 35 days post Mtb infection, when Mtb-specific T cell responses are already established in the lung as observed from 21 days post-Mtb infection (Fig. 3C, D), Gem had no detrimental effect on driving TB pathogenesis and hindering Th1 responses (Supplementary Fig. 14D–F). In summary, when Mtb-specific Th1 responses were already established, Gem did not mediate disease exacerbation, indicating that Gem-induced TB immunopathogenesis could be a consequence of the scarce presence of Mtb-specific T cells at a specific time point. Previously, our group reported that BCG vaccination significantly induced IFN-γ-producing Mtb-specific T cells in the lungs at 14 days post Mtb infection, a time when IFN-γ responses are barely elicited in mice infected only with Mtb[35]. To further investigate the effect of pre-existing Mtb-specific T cells on induced TB immunopathogenesis, mice were vaccinated with BCG at 56 days prior to Mtb infection to elicit memory responses against Mtb infection. Subsequently, BCG-vaccinated mice were infected with Mtb and administered with Gem 3 times at 2-day intervals, starting 13 days post-Mtb infection (Fig. 6A). Despite Gem treatment, BCG-vaccinated group displayed ameliorated lung inflammation and decreased bacterial loads both in the lungs and spleen at 28 days post Mtb infection compared to un-vaccinated group (Fig. 6B, C). Additionally, Gem-induced neutrophil infiltration in the lung was dramatically decreased upon BCG vaccination (Fig. 6D). Collectively, these data suggest that BCG vaccine-mediated pre-established Mtb-specific T cell responses overcome Gem-induced exacerbation of TB immunopathogenesis including enhanced neutrophilic inflammation and increased bacterial burden.

BCG vaccination regulates granulocyte-biased generation in the bone marrow and maintains Mtb-specific T cells response after Gem treatment

Given that patients diagnosed with both stage IV cancer and pulmonary TB showed increased neutrophil counts and decreased lymphocyte counts during anti-cancer drug treatment (Fig. 1A), we wondered the relationship between increased neutrophils and delayed Mtb-specific T cells. To further investigate the relationship, we first examined the bone marrow (BM) where hematopoietic stem cells (HSCs) reside, capable of regulating granulopoiesis by directly or indirectly sensing

https://doi.org/10.1038/s41467-025-63930-0

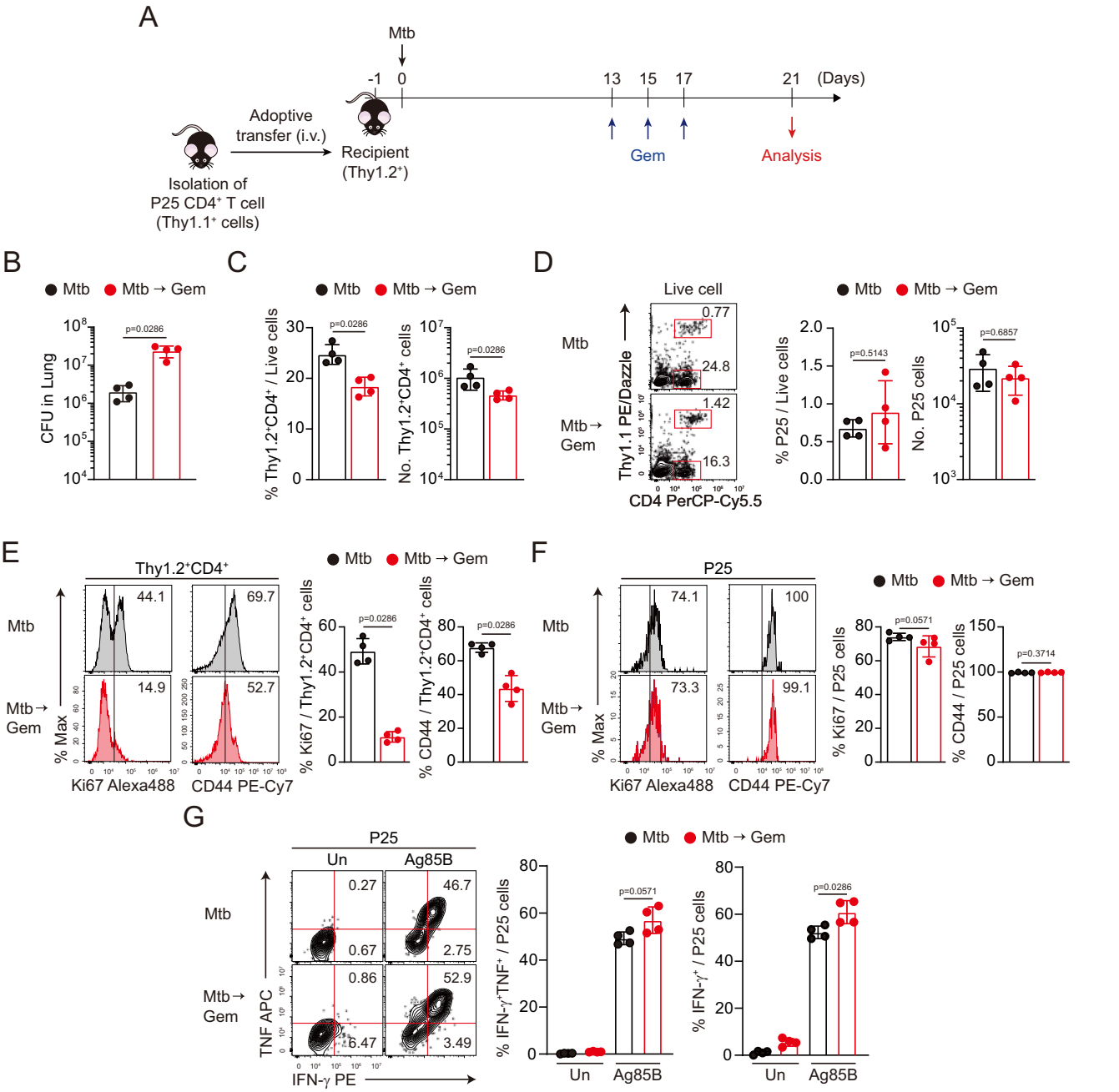

Fig. 5 | Preserved function and proliferation of adoptively transferred P25 CD4$^+$ T cells upon gemcitabine (Gem) treatment. A Naïve CD4$^+$ T cells were isolated from the spleens of P25 mice (Thy1.1$^+$) and adoptively transferred via i.v. injection to C57BL/6J naïve mice (Thy1.2$^+$). At 1 day after transfer, mice were infected with Mtb (~350 CFUs). **B** CFUs in the lungs at 21 days post Mtb infection ($n = 4$). The graph shows the mean ± SD. Data were analyzed by two-tailed Mann–Whitney rank test. **C**, **D** The frequency and number of Thy1.2$^+$ P25 cells or Thy1.1$^+$CD4$^+$ T cells among lung cells ($n = 4$). The graph shows the mean ± SD. Data were analyzed by two-tailed Mann–Whitney rank test. **E**, **F** The frequencies of Ki67$^+$ and CD44$^+$ cells among Thy1.2$^+$CD4$^+$ T cells or Thy1.1$^+$ P25 cells were analyzed by flow cytometry and are summarized in the graph ($n = 4$). The graph shows the mean ± SD. Data were analyzed by two-tailed Mann–Whitney rank test. **G** Isolated lung lymphocytes were restimulated ex vivo with Ag85B peptides, stained, and assessed for Thy1.1$^+$ P25 cells among lung cells ($n = 4$). The graph shows the mean ± SD. Two-tailed Mann–Whitney rank tests were used to compare groups. n.s. not significant, $^*p < 0.05$. **B**–**G** The data are representative of at least two independent experiments. Source data are provided as a Source Data file.

pathogens[36]. Gem treatment in Mtb-infected mice triggered the expansion of HSC progenitor lineage$^-$Sca-1$^+$c-Kit$^+$ (LSK$^+$) cell population along with the increase of granulocyte/macrophage progenitors (GMPs; lineage$^-$Sca-1$^-$c-Kit$^+$CD34$^+$CD16/32$^+$), whereas BCG vaccination prior to Mtb infection significantly reduced the frequency of progenitor cells, irrespective of Gem treatment (Fig. 7A and Supplementary Fig. 15). In addition, BCG vaccination strongly inhibited the increase of Sca-1$^+$ GMPs, which are reported to be more proliferative compared to GMPs and related to emergency myelopoiesis[43], in the Mtb-infected mice even after Gem treatment (Fig. 7A). Since G-CSF was upregulated in the serum of Mtb-infected and subsequent Gem-treated mice (Fig. 4I), we examined the level of G-CSF in the serum of BCG-vaccinated mice followed by Mtb infection and Gem treatment. Of interest, G-CSF production in the serum of Mtb-infected was significantly abrogated when preceded by BCG vaccination (Fig. 7B). STAT3 phosphorylation in bone marrow cells, which is the downstream

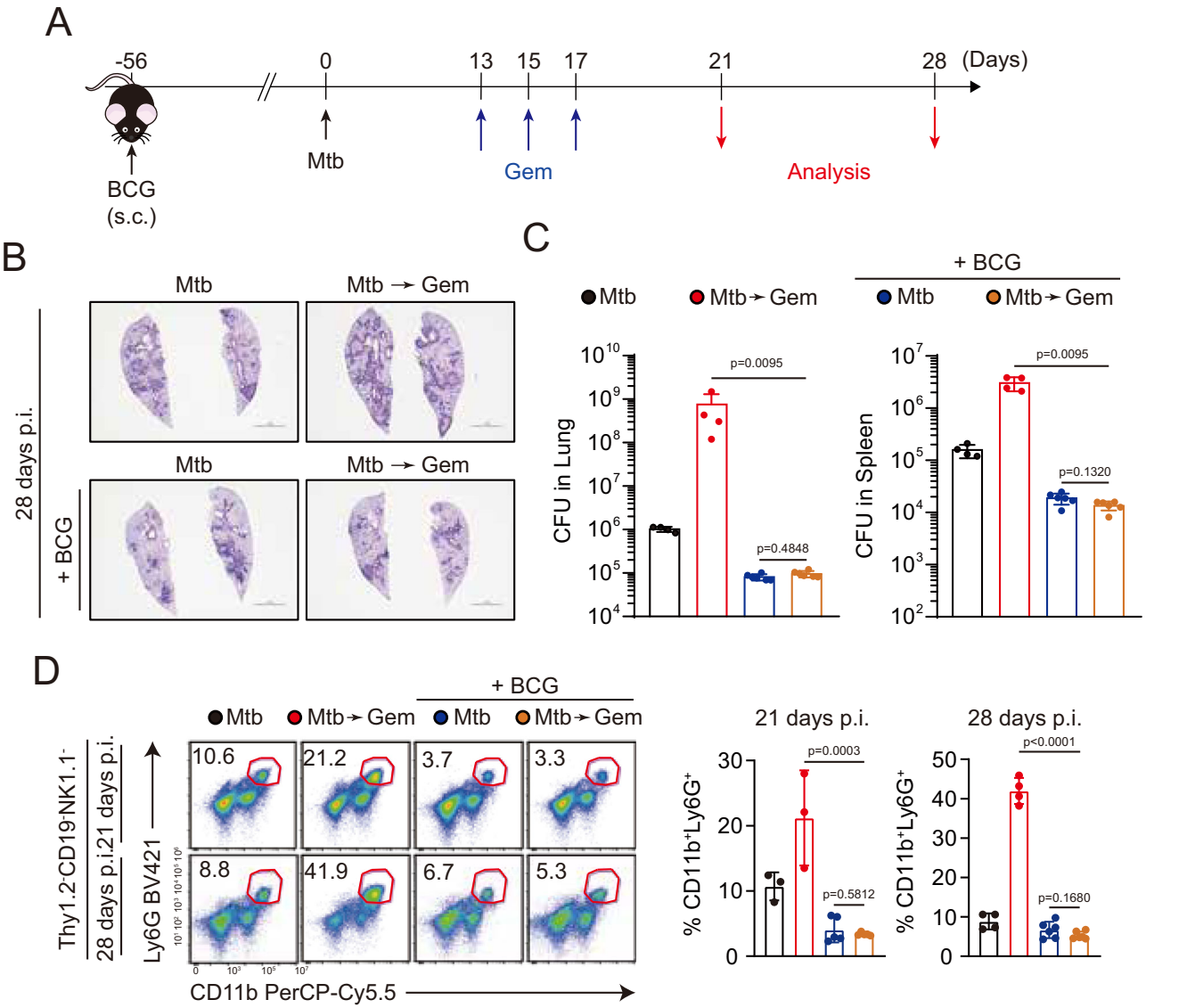

Fig. 6 | BCG vaccine-mediated protection in Mtb-infected mice followed by gemcitabine (Gem) treatment. A C57BL/6J mice were vaccinated 56 days before challenge with Mtb. **B** H&E staining of lungs in each group (10×, scale bars = 2.0 mm). **C** Bacterial loads in the organs of each group. ($n = 4, 6$). The graph shows the mean ± SD. Two-tailed Mann–Whitney rank tests were used to compare groups. $^{**}p < 0.01$. **D** The frequency of $CD11b^+Ly6G^+$ cells. The numbers in the plot indicate the percentage of cells ($n = 3, 4, 6$). The graph shows the mean ± SD. Data were analyzed by two-tailed unpaired *t*-test. $^{***}p < 0.001$, and $^{****}p < 0.0001$ between group. **B**–**D** The data are representative of at least two independent experiments. Source data are provided as a Source Data file.

event of G-CSF receptor signaling[36], was also significantly decreased in Gem-treated mice by BCG vaccination (Fig. 7C). Moreover, BCG vaccination even after Gem treatment of Mtb-infected mice maintained the number of Mtb-specific $CD4^+$ T cells capable of producing IFN-γ upon restimulation of lung cells with purified protein derivative (PPD) (Fig. 7D). It is worthwhile to note that $CD4^+$ T cell-derived IFN-γ also tended to increase upon restimulation with ESAT-6 ($p = 0.0712$), which BCG does not harbor[44], in the BCG-vaccinated mice post Mtb infection even after Gem treatment (Fig. 7D). These data indicate that Gem-induced TB exacerbation was abrogated by the presence of pre-existing Mtb-specific T cell responses at the time of Gem treatment.

G-CSF neutralization restricts Gem-induced neutrophilic inflammation during TB

To further confirm G-CSF as a causative cytokine for Gem-induced neutrophilic inflammation, we administered an anti-G-CSF antibody to Gem-treated mice starting at 13 days post-Mtb infection, every alternate day till day 27 via intraperitoneal route. Notably, Gem-induced TB exacerbation, characterized by pulmonary inflammation, was significantly ameliorated upon G-CSF neutralization in Gem-treated mice compared to those treated with an isotype control (Fig. 8A, B). Additionally, G-CSF neutralization prevented weight loss in Gem-treated mice and mediated a significant reduction in bacterial load compared to those treated with an isotype control at 28 days post-Mtb infection (Fig. 8C, D). Moreover, Gem-induced neutrophil infiltration in the lung was significantly decreased upon G-CSF neutralization, accompanied by reduced expression of ARG1 among neutrophils (Fig. 8E and Supplementary Fig. 16A). In line with this, Gem-triggered increase in the frequency of both GMPs and $Sca\text{-}1^+$ GMPs in bone marrow was mitigated by targeting G-CSF, except for LSK^+ cell population, whose frequency was increased (Fig. 8F). Although improved protection was mediated upon G-CSF neutralization in Gem-treated mice, as observed in neutrophil depletion (Fig. 4H), restored numbers and responses of Mtb-specific T cells were still not observed at 21 days post Mtb infection (Fig. 8G and Supplementary Fig. 16B). In summary, the increase in G-CSF following Gem treatment during TB exacerbates disease progression by driving

https://doi.org/10.1038/s41467-025-63930-0

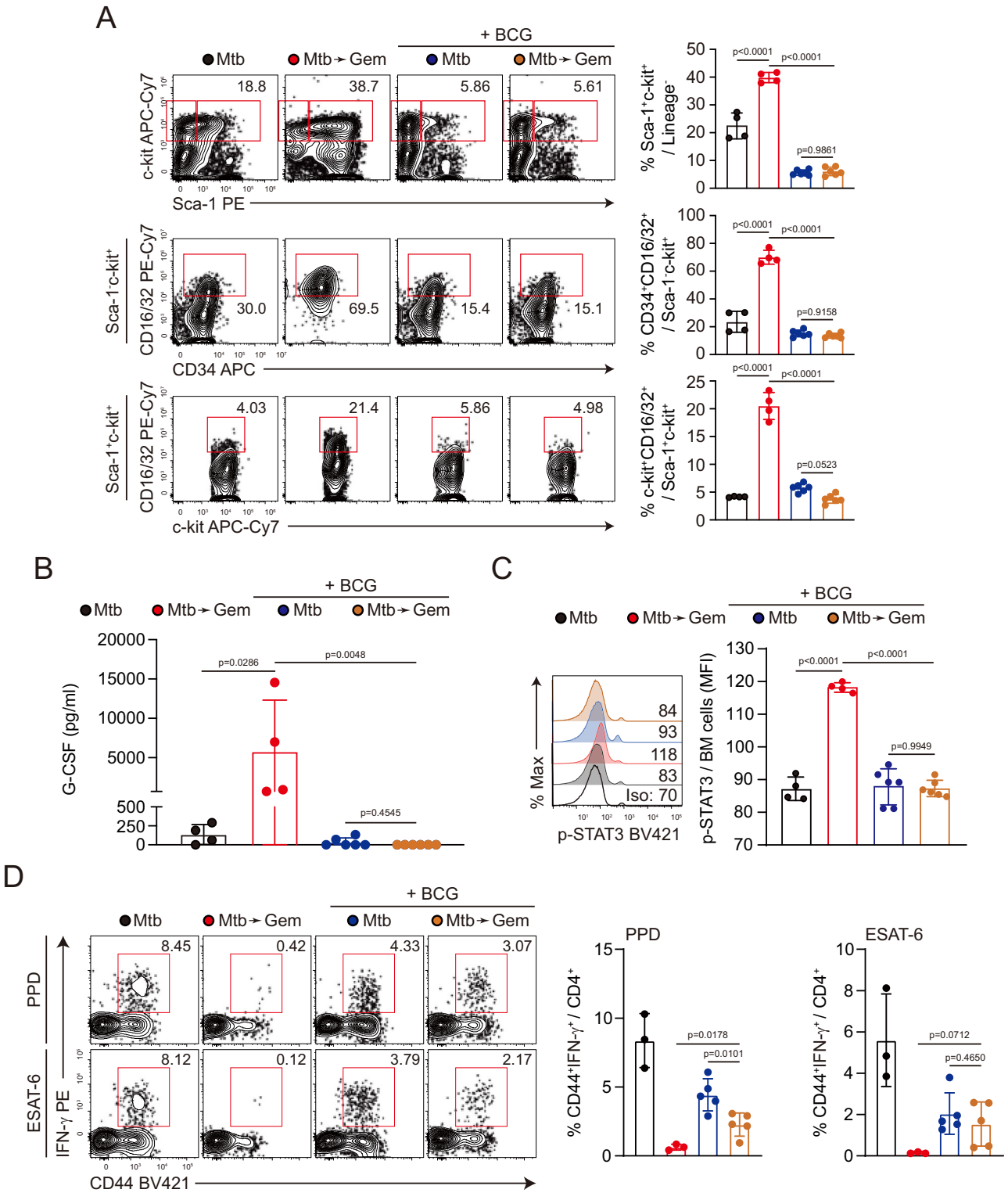

Fig. 7 | Analysis of bone marrow and Mtb-specific T cells after treatment of gemcitabine (Gem) in BCG-vaccinated mice during Mtb infection. **A** Representative flow cytometry plots and the frequencies of lineage$^-$Sca-1$^+$c-Kit$^+$ (LSK$^+$), lineage$^-$Sca-1$^-$c-Kit$^+$CD34$^+$CD16/32$^+$, lineage$^-$Sca-1$^+$c-kit$^+$CD16/32$^+$ cell population at 28 days post Mtb infection ($n = 4$ and 6). The graph shows the mean ± SD. Data were analyzed by one-way ANOVA with post hoc Tukey test. **B** The level of G-CSF in serum were analyzed by ELISA ($n = 4$ and 6). The graph shows the mean ± SD. Two-tailed Mann–Whitney rank tests were used to compare groups. n.s. not significant, $^*p < 0.05$, and $^{**}p < 0.01$. **C** Phosphorylation of STAT3 was analyzed in the bone marrow cells at 28 days post Mtb infection ($n = 4$ and 6). Data were analyzed by one-way ANOVA with post hoc Tukey test. The graph shows the mean ± SD. n.s. not significant and $^{****}p < 0.0001$. **D** The number of IFN-γ- and TNF-producing CD4$^+$ T cells were analyzed by flow cytometry ($n = 3$ and 5). The graph shows the mean ± SD. Data were analyzed by two-tailed unpaired *t*-test. n.s. not significant and $^*p < 0.05$ between group. **A**–**D** The data are representative of at least two independent experiments. Source data are provided as a Source Data file.

granulopoiesis-induced neutrophilic inflammation, without directly impacting delayed Mtb-specific T cell responses.

IFN-γ neutralization reverses the protective effect of BCG vaccine against Gem-induced TB exacerbation

Considering that BCG conferred protection against Gem treatment, evidenced by decreased generation of neutrophils and production of G-CSF, along with an unaffected IFN-γ-producing Mtb-specific CD4$^+$ T cell response (Figs. 6 and 7), we further examined the impact of IFN-γ on BCG-mediated control of Gem-induced TB exacerbation. To this end, BCG-vaccinated mice followed by Mtb infection and Gem treatment were administered with anti-IFN-γ antibody, starting at 6 days post infection, every alternate day till day 16. via intraperitoneal route. Importantly, BCG vaccination did not confer protection against Gem

Fig. 8 | Improved protection without restoration of Mtb-specific T cell responses in gemcitabine (Gem)-treated mice upon G-CSF neutralization. **A** Gross pathology or H&E staining of lungs in each group. ($n = 5$) (10×, scale bars = 2.0 mm). **B** The data represent the percentages of the superior lobe of the right lung showing inflammation ($n = 5$). The graph shows the mean ± SD. Two-tailed Mann–Whitney rank tests were used to compare groups. n.s. not significant and $^{**}p < 0.01$. **C** The weight of mice at the indicated time points ($n = 5$). The graph shows the mean ± SD. Data of 28 days post-Mtb infection were analyzed by two-way ANOVA with post hoc Tukey's test. n.s. not significant and $^{*}p < 0.05$. **D** Bacterial loads in the organs of each group ($n = 5$). The graph shows the mean ± SD. Two-tailed Mann–Whitney rank tests were used to compare groups. $^{**}p < 0.01$. **E** The frequency and number of $CD11b^{+}Ly6G^{+}$ cells. The numbers in the plot indicate the percentage of cells ($n = 5$). The graph shows the mean ± SD. Data were analyzed by one-way ANOVA with post hoc Tukey test. **F** Representative flow cytometry plots and the frequencies of $lineage^{-}Sca\text{-}1^{+}c\text{-}Kit^{+}$ (LSK^{+}), $lineage^{-}Sca^{-}1^{-}c\text{-}Kit^{+}CD34^{+}CD16/32^{+}$, $lineage^{-}Sca^{-}1^{+}c\text{-}kit^{+}CD16/32^{+}$ cell population at 28 days post Mtb infection ($n = 5$). The graph shows the mean ± SD. Data were analyzed by one-way ANOVA with post hoc Tukey's test. **G** The frequencies and numbers of $ESAT6_{4\text{-}17}$:I-A(b)- or $Ag85B_{280\text{-}294}$:I-A(b)-specific $CD4^{+}$ T cells identified by tetramer staining were analyzed by flow cytometry. The numbers in the plots indicate the percentage of tetramer-positive cells among $CD4^{+}$ T cells ($n = 5$). The graph shows the mean ± SD. Data were analyzed by one-way ANOVA with post hoc Tukey's test. **A**–**G** The data are representative of at least two independent experiments. Source data are provided as a Source Data file.

treatment in Mtb-infected mice upon IFN-γ neutralization, as evidenced by significantly increased pulmonary inflammation and bacterial loads in the lungs at 28 days post infection, compared to the isotype-treated group (Fig. 9A–C). Aligned with the regained severe phenotype, neutrophils that had been decreased by BCG vaccination were observed to increase again in response to Gem treatment at 21 and 28 days post-Mtb infection upon IFN-γ neutralization (Fig. 9D). Additionally, IFN-γ-producing Mtb-specific $CD4^{+}$ T cells upon PPD stimulation were not affected in BCG-vaccinated mice against Gem treatment irrespective of IFN-γ neutralization (Fig. 9E). Furthermore, IFN-γ neutralization significantly elicited increased production of G-CSF in the serum of BCG-vaccinated mice compared to the isotype-treated group (Fig. 9F). Taken together, our data demonstrate that IFN-γ neutralization is sufficient to significantly abrogate BCG vaccination-derived protection, suggesting that Gem-driven neutrophilic inflammation occurred in the absence of IFN-γ and that IFN-γ might mediate its protective effect precisely at the time of Gem treatment during TB, by restricting G-CSF production and subsequent granulocyte-biased generation in the bone marrow against Gem-induced TB immunopathogenesis.

Discussion

In this study, we used a mouse model of Mtb infection treated with anti-cancer drugs to assess how these drugs affect tuberculosis (TB) progression. We found that anti-cancer drug treatment can worsen TB immunopathogenesis as an independent risk factor by mediating permissive neutrophilic inflammation following the scarce presence of T cells. The neutrophil-to-lymphocyte (N:L) ratio, easily measured from routine blood tests, helps gauge inflammation[45]. It is linked to prognosis in cancer, cardiovascular, rheumatic, and infectious diseases[46–48], including TB. In TB, a high N:L ratio predicts active disease risk and severity[49–51]. Our data show that cancer patients progressing to active TB after anti-cancer drug treatment have increased neutrophils and reduced lymphocytes (Fig. 1A). Since anti-cancer drugs may cause neutropenia and raise infection risk, G-CSF is used preventively[52–54]. However, our analysis excluded patients treated with G-CSF (Supplementary Fig. 1). Nevertheless, patients with active TB exhibited neutrophilia along with decreased lymphocytes.

Using an experimental murine model, we found that treatment with anti-cancer drugs such as Gem, CP, and PTX exacerbated TB immunopathogenesis (Fig. 2 and Supplementary Fig. 6). This was evidenced by increased neutrophil presence and diminished Mtb-specific T cell responses in the lungs (Figs. 2 and 3). Previous research demonstrated that Gem was used to deplete granulocyte precursors in Mtb-infected $Nos2^{-/-}$ mice, and its treatment tended to reduce neutrophils accompanied by bacterial decrease in the lungs[29]. Intriguingly, in our model, Mtb-infected mice displayed an increase in neutrophils accompanied by elevated bacterial burdens in the lungs following Gem treatment (Fig. 2C–E). This may be because the pathogenesis in C57BL/6J wildtype mice is not solely mediated by neutrophils, as these mice showed resistance against Mtb infection compared to the TB-susceptible $Nos2^{-/-}$ mice, where a significant increase in neutrophils was observed only in $Nos2^{-/-}$ mice[29]. Thus, notably, the immunopathology mediated by anti-cancer drugs during TB infection differs immunologically depending on the mouse model used. Nevertheless, both studies identified that neutrophil accumulation in the lungs of Mtb-infected mice is a main hallmark of the progression to severe TB, regardless of the mice's susceptibility to Mtb infection.

In both human patients and various susceptible mouse strains, a significant characteristic of severe TB is the influx of granulocytic cells, particularly neutrophils, into the lungs. Although neutrophil recruitment is crucial for immune defense against many lung infections, and some animal studies suggest that neutrophils may offer protection during the initial phases of mycobacterial infections[55–58], extensive evidences from both human cases and susceptible mice indicate that these cells contribute to TB pathology[24,27–30,59]. Together with neutrophil manifestation, delayed Mtb-specific T cell responses, which play a crucial role in protecting the host against infections[35], were significantly observed at 21 days post-Mtb infection in Gem-treated mice, exhibiting signs of recovery by 28 days post-Mtb infection (Fig. 3). Considering that the rapid migration of Mtb-specific T cells to the lung is important for Mtb control[35,60,61], and that this delay might be the cause of neutrophil accumulation[62], we initially targeted neutrophils with the anti-1A8 antibody to identify the relationship between neutrophilia and delayed Mtb-specific T cell responses. Upon neutrophil depletion, we observed a reduction in pulmonary inflammation and bacterial loads, accompanied by decreased levels of pro-inflammatory cytokines in the serum and lung lysates of Mtb-infected mice following Gem treatment (Fig. 4). Interestingly, a pronounced restoration of IFN-γ in lung lysates was measured upon neutrophil depletion at 28 days post-Mtb infection, compared to the Gem-treated isotype control group. However, Mtb-specific T cell responses were still delayed at 21 days post-Mtb infection (Fig. 4G, H), suggesting the suppressive contribution of neutrophils on T cells. Neutrophils in the Gem-treated group exhibited increased expression of ARG1 and Nos2 (Supplementary Fig. 11A), which are distinct characteristics of MDSCs[39,63,64]. However, the suppression experiments indicated that Gem-induced neutrophils were not suppressive to T cells (Supplementary Fig. 11D). This may be because the suppression experiment conducted ex vivo might not fully reflect the in vivo environment of Gem-treated mice. In addition, neutrophils observed at 28 days post-Mtb infection might be involved in driving TB pathogenesis afterwards as MDSCs by acquiring coexpression of ARG1 and Nos2, although we did not assess this further. Instead, to explain this delay, and given that the abundance and T cell positioning in TB lesions are important for Mtb control, neutrophils could play a role in interfering with T cell responses or their interaction with infected phagocytes[65], resulting in the differential extent of restoration. These findings indicate that increased neutrophils are more likely to be a consequence of delayed Mtb-specific T cell responses and are the main culprits driving Gem-induced TB immunopathology.

Then, we sought to elucidate the relationship between Gem treatment and Mtb-specific T cells. For this purpose, P25 T cells were adoptively transferred and analyzed post-Gem treatment. Intriguingly,

https://doi.org/10.1038/s41467-025-63930-0

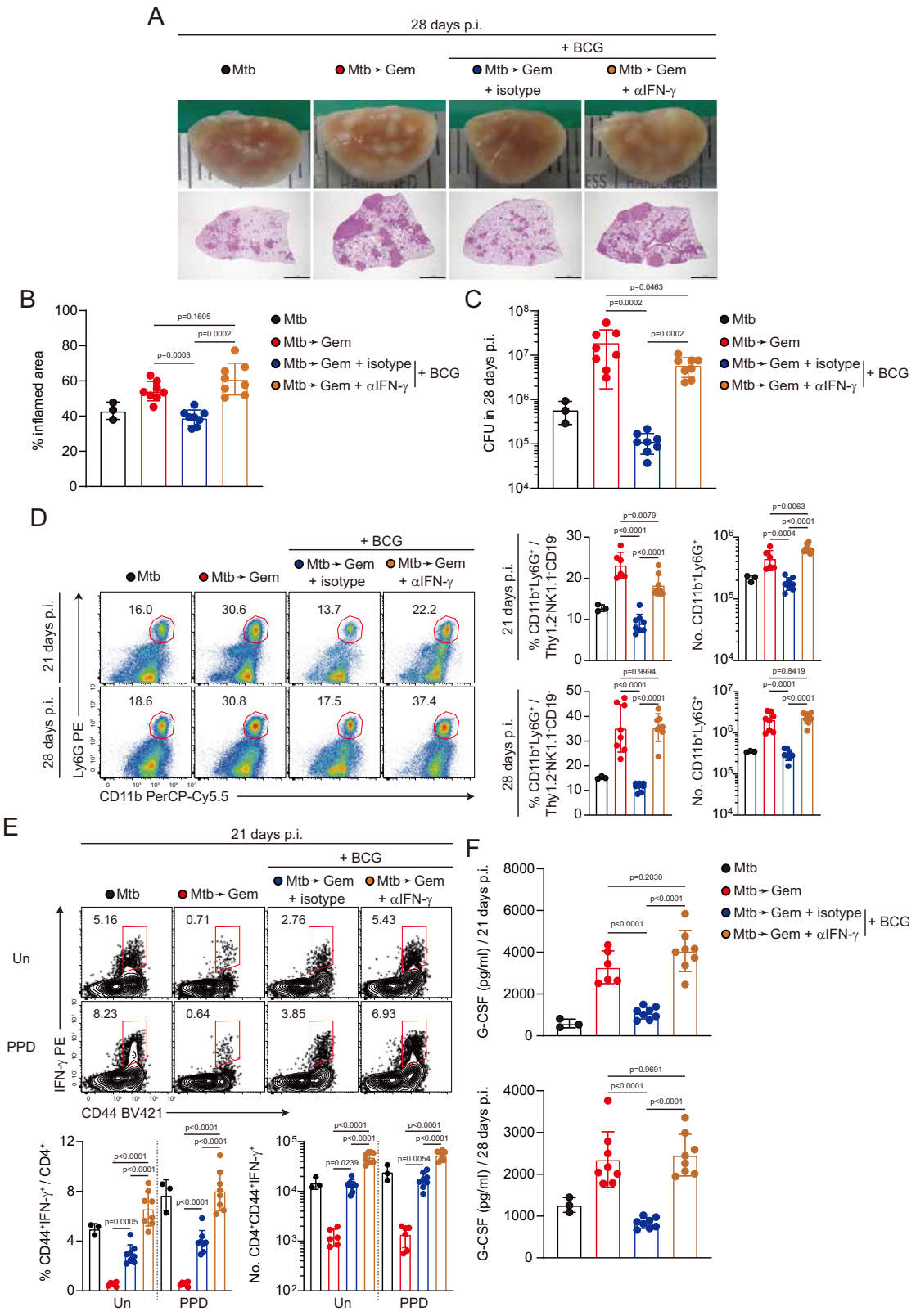

the proliferation, activation, and functionality of P25 T cells in the lungs were preserved upon Gem treatment, while these parameters were significantly curtailed in recipient CD4$^+$ T cells (Fig. 5), suggesting that Gem may induce delayed Mtb-specific T cell responses by affecting the priming and clonal expansion of these T cells. Together with Gem treatment at 5 weeks and BCG vaccination experiments (Fig. 6 and Supplementary Fig. 9), it seems plausible that neutrophil manifestation occurs in the absence of Mtb-specific T cells, and Gem exacerbates disease severity when administered at specific time points during the generation of Mtb-specific T cells. In addition, Gem treatment during Mtb infection may affect TB progression due to dysregulated hematopoiesis in the bone marrow. Indeed, increased production of G-CSF triggered its downstream STAT3 phosphorylation accompanied by expansion of LSK and GMP populations (Fig. 7A–C),

Fig. 9 | Exacerbated TB progression in BCG-vaccinated mice after Gem treatment upon IFN-γ neutralization. A Gross pathology or H&E staining of lungs in each group. ($n = 3, 8, 8, 8$) (10×, scale bars = 2.0 mm). **B** The data represent the percentages of the superior lobe of the right lung showing inflammation ($n = 3, 8, 8, 8$). The graph shows the mean ± SD. Data were analyzed by two-tailed Mann–Whitney rank test. **C** Bacterial loads in the organs of each group ($n = 3, 8, 8, 8$). The graph shows the mean ± SD. Two-tailed Mann–Whitney rank tests were used to compare groups. n.s. not significant, $^{*}p < 0.05$, and $^{***}p < 0.001$. **D** The frequency and number of $CD11b^{+}Ly6G^{+}$ cells. The numbers in the plot indicate the percentage of cells ($n = 3, 8, 8, 8$). The graph shows the mean ± SD. Data were analyzed by one-way ANOVA with post hoc Tukey test. **E** The frequency and number of IFN-γ- and TNF-producing $CD4^{+}$ T cells were analyzed by flow cytometry ($n = 3, 8, 8, 8$). The graph shows the mean ± SD. Data were analyzed by one-way ANOVA with post hoc Tukey test. **F** The level of G-CSF in serum were analyzed by ELISA ($n = 3, 8, 8, 8$). The graph shows the mean ± SD. Data were analyzed by one-way ANOVA with post hoc Tukey's test. The data are representative of a single experiment. Source data are provided as a Source Data file.

indicating a bias towards granulopoiesis. This was evidenced by Gem-induced neutrophilic inflammation with delayed Mtb-specific T cell responses in Mtb-infected mice, reflecting patients diagnosed with both stage IV cancer and pulmonary TB. Furthermore, G-CSF neutralization remarkably prevented Gem-induced neutrophilic inflammation, accompanied by reduced expansion of GMP and $Sca\text{-}1^{+}$ GMP populations (Fig. 8), indicating decreased granulocyte-biased generation. Additionally, in line with observations of neutrophil depletion, G-CSF neutralization had no effect on the restoration of Mtb-specific T cell responses (Fig. 8G). However, when BCG vaccination was preceded, Mtb-infected mice followed by Gem treatment displayed no exacerbation of Gem-induced neutrophilic inflammation in the lung accompanied by preserved Mtb-specific T cell responses (Figs. 6 and 7D). Consistent with this, it has been reported that IFN-γ suppressed the activation of G-CSF-induced essential transcription factor for emergent granulopoiesis, STAT3, by induing the expression of SOCS3[66]. In addition, IFN-γ-deficient mice displayed increased neutrophils upon infections[66–70]. This was further supported by our observations that IFN-γ neutralization significantly abrogated the protection in BCG-vaccinated mice without neutrophilia and increased G-CSF (Fig. 9). Several studies have reported that G-CSF contributes to inhibition of T cell responses apart from induction of neutrophilic inflammation[71–73]. However, in our study, the contribution of G-CSF to delayed Mtb-specific T cell responses seems different in that this delay could be caused by the reconstitution of cell populations towards the expansion of granulocytes, such as decreased dendritic cells, after treatment with Gem, rather than by the direct G-CSF-G-CSFR signaling pathway. Moreover, the treatment of Gem could cause different consequences depending on the presence of IFN-γ. In summary, IFN-γ could mediate its protective effect precisely at the time of Gem treatment during TB, by limiting G-CSF production and subsequent granulocyte-biased hematopoiesis.

Our current study has certain limitations that require further consideration. Firstly, in a real-world setting, neither neutrophilia nor aggravation of TB was observed in a subset of patients ($n = 9$). Several plausible reasons could explain these contradictory results. One possibility is the ineffective myelopoiesis due to bone marrow invasion by cancer cells. Mouse models of prostate cancer with bone marrow involvement have demonstrated that cancer cells competed with HSCs for occupancy in the HSC niche[74]. Once in the niche, cancer cells displace HSCs, substantially reducing their numbers[75]. This displacement might compromise myeloid cell production, resulting in myeloid cells with functional defects[76]. Another potential explanation involves the long duration of treatment and multiple anti-cancer drug regimens, particularly in heavily treated cancer patients whose myelopoiesis is altered by chemotherapy, rendering them immunocompromised[77]. Additionally, a large tumor burden may lead to failures in the ability of myeloid cells to act as professional antigen-presenting cells (APCs), which are essential for eliciting tumor-specific responses necessary to combat cancer cells and infections[78,79]. It is possible that patients who exhibited neutrophilia had relatively more functional APCs. Further studies are needed to elucidate the relationship between myeloid dysfunction and TB in patients with advanced, metastatic cancer. Then, to explore potential differences between patients with and without neutrophilia, we compared several demographic and clinical factors between the two groups; no significant differences were observed. However, a higher proportion of patients who developed neutrophilia had strong AFB positivity (AFB 3+ or 4+, 6/7 patients) compared to those without neutrophilia (4/9 patients) (Supplementary Fig. 3). Given the retrospective nature of the study, we acknowledge that these findings may be influenced by unmeasured confounding factors. Secondly, while using an experimental murine model, we did not employ a cancer-injected mouse model that perfectly reflects patient conditions. Rather, our study focused on analyzing the pathogenic role of anti-cancer drugs during TB as an independent contributing factor, considering that the presence of old-healed TB was associated with TB reactivation during anti-cancer drug treatment[80]. However, we observed apparent disease progression when mice were infected with a low dose of Mtb, although not with an ultra-low dose, which more closely resembles the human reactivation model[81]. We believe that experiments with ultra-low dose infections of Mtb could provide deeper insights into the mechanisms underlying the development of active TB during anti-cancer treatment. Additionally, this experimental mouse model was based on clinical observations of an anecdotal phenomenon where TB appeared to be aggravated in patients with solid tumors undergoing chemotherapy. Due to the nature of this phenomenon, conducting a well-designed prospective study and developing a mouse model that reflects the exact clinical situation have limitations. In contrast to mice, it is difficult to determine whether proper adaptive immunity to Mtb is established in patients. Moreover, there are no specific guidelines for screening or treating latent TB infection (LTBI) in patients with cancer[10]. Nevertheless, our model demonstrated that neutrophils are the main culprits driving TB immunopathogenesis when proper adaptive immunity to Mtb is delayed. This reflects the findings in 7 of 16 patients, who exhibited increased neutrophils accompanied by decreased lymphocytes following treatment with anti-cancer drugs. Thirdly, there was a significant decrease in $CD11b^{+}F4/80^{+}$ macrophages at 28 days post-infection (Fig. 2E). Since necrosis has been regarded as a pathway for granuloma cavity formation and bacterial dissemination[82], the death of macrophages upon Gem treatment might contribute to disease progression accompanied by neutrophilia, although we did not investigate this further. Fourthly, regarding the restoration of dysregulated hematopoiesis upon BCG vaccination, the protective contribution of BCG-derived trained immunity and alteration of early myeloid cell responses should not be overlooked. BCG vaccination may induce trained immunity through the education of HSCs or generation of IFN-γ producing $CX3CR1^{hi}$ effector memory T cells[83,84]. However, both studies observed that BCG-induced trained immunity was initiated when BCG was administered via intravenous route, not subcutaneous route. In addition, BCG vaccination-derived $CX3CR1^{hi}$ effector memory T cells provided cross protection based on enhanced antimicrobial activity of alveolar macrophages in IFN-γ dependent manner[84]. On the other hand, BCG immunization could shape early myeloid cell responses in the lung, resulting in protection by recruiting monocyte-derived macrophages and neutrophils. This recruitment is likely related to IFN-γ[42]. Thus, in addition to the regulatory effect of IFN-γ in limiting neutrophilic inflammation, its protective role in the contribution of T cells and infected cells, based on the alteration of myeloid cell responses in the lung, should be further

considered upon IFN-γ neutralization in BCG-immunized mice. Nevertheless, in the current study, we highlighted that BCG vaccination-derived IFN-γ-producing Mtb-specific T cells may help mediate protection by counteracting the granulopoiesis bias under anti-cancer treatment during TB. Apart from BCG vaccination, it might be worthwhile to see whether adoptive transfer of $CD4^+$ T cells purified from vaccinated mice could Gem-induced TB immunopathology in $CD4^+$ T cell depleted mice, by emphasizing the protective role of Mtb-specific T cells in different way. Lastly, we commonly observed severe TB phenotypes upon treatments of three anti-cancer drugs. Then, we determined to use Gem in subsequent experiments, as it was administered to the majority of patients and demonstrated more pronounced effects on lung inflammation and bacterial loads in Mtb-infected mice compared to PTX or CP. Nevertheless, further studies are required to clarify whether other anti-cancer drugs could induce TB immunopathogenesis in same manner.

In summary, anti-cancer drug treatment during Mtb infection leads to TB immunopathogenesis by promoting neutrophilic inflammation in the lung. The immunopathological characteristics were diminished by neutrophil depletion, G-CSF neutralization, and BCG vaccination, highlighting that treatment of anti-cancer drug has different consequences depending on the presence or timing of IFN-γ. Thus, our current study demonstrates the pathogenic function of anti-cancer drugs during Mtb infection and suggests that eliciting Mtb-specific T cells through vaccination may be an effective prophylactic strategy to protect the host from the immunomodulatory effects of such drugs in the context of TB based on counteracting granulopoiesis bias.

Methods

Study approval

Data of patients was approved by institution review board of Yonsei Cancer Center (Permit Number: 4-2020-0266). All animal studies were performed in accordance with Korean Food and Drug Administration (KFDA) guidelines. The experimental protocols used in this study were reviewed and approved by the Ethics Committee and Institutional Animal Care and Use Committee (Permit Number: 2020-0103) of the Laboratory Animal Research Center at Yonsei University College of Medicine (Seoul, Korea).

Selection criteria of patients

Data of patients who were positive for Mtb ($n = 2533$) in Severance Hospital from January 2005 to July 2019 were obtained (Supplementary Fig. 1). Patients who were (1) not diagnosed with cancer ($n = 1990$), and (2) had no exposure to chemotherapeutic agents ($n = 449$) such as Gem, CP, and PTX were excluded. Key inclusion criteria for patient selection was time frame of within 1 year during chemotherapy and tuberculosis medication. Patients who were (1) treated with chemotherapy before or after 1 year ($n = 63$), (2) patients who did not receive anti-tuberculosis treatment ($n = 11$), and (3) patients who were treated with granulocyte-colony stimulating factor (G-CSF) ($n = 3$) were excluded since G-CSF stimulates bone marrow to produce granulocytes, including neutrophils. Of the 16 patients selected, 7 patients showed neutrophilia with the following chemotherapies: Gem ($n = 10$), CP ($n = 1$), Gem and CP ($n = 2$), and CP and PTX ($n = 2$), while 9 patients did not. Comparative demographic and clinical data between these two groups are provided in Supplementary Tables 1 and 2, respectively. Furthermore, to demonstrate the representative patterns of neutrophilia associated with TB exacerbation, three cases from the neutrophilia group were selected. The other four patients did not show TB exacerbation based on chest X-ray imaging. Detailed longitudinal laboratory trends for these three representative patients are illustrated in Fig. 1B–D.

Animals

Specific pathogen-free female C57BL/6J (6–7 weeks old) were purchased from Japan SLC, Inc. (Shizuoka, Japan), and maintained under barrier conditions in the ABSL-3 facility at the Yonsei University College of Medicine. P25 (C57BL/6-Tg (H-2Kb-Tcra,Tcrb)P25Ktk/j) (The Jackson Laboratory, JAX:011005) mice were purchased from Jackson Laboratory (Bar Harbor, ME). Thy1.1-expressing congenic C57BL/6J mice were generously provided by Rafi Ahmed of Emory University (Atlanta). Ly5.1 mice (B6.SJL-Ptprca Pep3b/BoyJ) (The Jackson Laboratory, JAX:002014) were obtained from laboratory of Young-Chul Sung (POSTECH, Republic of Korea). These two strains were mated to generate $Thy1.1^+$ P25 or $Ly5.1^+$ P25 mice. All mice were housed in a constant temperature/humidity environment (24 ± 1 °C, 50 ± 5%) under light-controlled conditions (12 h light-dark cycle; 7 a.m. on and 7 p.m. off) and fed a sterile commercial mouse diet with *ad libitum* access to water. Then, the mice were euthanized via CO_2 asphyxiation at the experimental endpoints.

Preparations of Mtb strains

Mtb K strain was obtained from the strain collections at the Korean Institute of Tuberculosis (KIT, Osong, Chungchungbuk-do, Korea). *M. bovis* BCG (Pasteur strain 1173P2) was kindly provided by Dr. Brosch at the Pasteur Institute (Paris, France). All mycobacteria used in this study were prepared as described previously[35].

Infection and treatment of anti-cancer drugs

Mice were aerogenically challenged with Mtb K strain as previously described[35]. Aerosol infection was performed using a Glas-Col aerosol apparatus (Terre Haute, IN, USA) adjusted to achieve a predetermined dose of approximately 200 to 300 viable bacteria. For instances of low dose or high dose infections that fall outside this range, details are specified in each figure legend. Anti-cancer drugs, including Gem, CP, and PTX were purchased from Sigma Aldrich (MO, USA). For treatment of anti-cancer drugs, Gem and CP were reconstituted with PBS. PTX was reconstituted with DMSO, ensuring that the final concentration of DMSO was 0.5% (vol/vol). Then, Gem (120 mg/kg), CP (3 mg/kg), or PTX (10 mg/kg) was treated through three intraperitoneal injections given 2 days apart starting at 2 weeks after aerosol Mtb infection. For determining time-dependent effect of Gem, drug was treated through three intraperitoneal injections given 2 days apart starting at 5 weeks after aerosol Mtb infection. For the vehicle control, Mtb infection only group was treated with PBS or with DMSO only when PTX treatment was conducted concurrently.

Bacterial enumeration and histopathology

To enumerate the number of bacteria, mice were euthanized with CO_2, and lungs and spleens were homogenized. The number of viable bacteria was determined by plating serial dilutions of the organ homogenates onto Middlebrook 7H10 agar (Difco, Detroit, MI, USA) supplemented with 10% OADC (Difco) and amphotericin B (Sigma-Aldrich, MO, USA). Colonies were counted after 4 weeks of incubation at 37 °C. For histopathological analysis, the middle cross-section from entire superior lobes of the right lung were collected, preserved in 10 % neutral buffered formalin overnight, embedded in paraffin, sectioned at 4–5 µm, and stained with hematoxylin and eosin (H&E), acid-fast bacilli (AFB) straining or bacilli rhodamine staining. The level of inflammation in the lungs was evaluated using by ImageJ (National Institutes of Health, USA) program, as previously described[2].

Flow cytometry and intracellular cytokine staining

For phenotypic analysis, single cell suspensions (1.0×10^6 cells) from the lungs of each group were first washed with 2% FBS containing PBS and blocked with anti-CD16/32 (BD Biosciences, San Jose, CA, USA) at 4 °C for 20 min. After the cells were stained with LIVE/DEAD Fixable Viability Dye (Thermo Fisher Scientific, Waltham, MA, USA), stained with fluorochrome-conjugated antibodies for 20 min at 4 °C. Fluorochrome-conjugated antibodies against CD11b (M1/70; 1:500 dilutions), Ly6G (1A8; 1:300 dilutions), Ly6C (AL-21; 1:300 dilutions),

F4/80 (T45-2342; 1:200 dilutions), CD90.2 (53-2.1; 1:300 dilutions), MHC Class II (M5/114.15.2; 1:300 dilutions), and NK1.1 (PK136; 1:300 dilutions) were obtained from BD Bioscience; antibodies against CD16/32 (93; 1:200 dilutions), CD19 (eBio1D3; 1:300 dilutions), Sca-1 (D7; 1:200 dilutions), CD117 (2B8; 1:200 dilutions), Arginase1 (A1exF5; 1:200 dilutions), and Nos2 (CXNFT; 1:200 dilutions) were obtained from ThermoFisher Scientific; antibodies against CD11c (N418; 1:300 dilutions), CD34 (MEC14.7; 1:200 dilutions), CD90.1 (OX-7; 1:200 dilutions), CD45 (30-F11; 1:300 dilutions), CD4 (RM4-5; 1:300 dilutions), CD45.1 (A20; 1:200 dilutions), CD8 (53-6.7; 1:300 dilutions), CD44 (IM7; 1:300 dilutions), Ki67 (16A8; 1:100 dilutions), and p-STAT3 (Tyr705; 13A3-1; 1:100 dilutions) were obtained from Biolegend (San Diego, CA, USA). The following antibodies were used for bone marrow cell staining: biotin-conjugated hematopoietic lineage labeling cocktail and anti-biotin (1:100 dilutions; Miltenyi Biotec, Bergisch Gladbach, Germany); biotin-conjugated antibodies against TER-119 (TER-119; 1:200 dilutions), CD11b (M1/70; 1:500 dilutions), CD5 (53-7.3; 1:200 dilutions), CD4 (RM4-5; 1:300 dilutions), CD8 (53-6.7; 1:300 dilutions), CD45R (RA3-6B2; 1:300 dilutions), Gr-1 (RB6-8C5; 1:300 dilutions), and fluorochrome-conjugated anti-streptavidin (1:200 dilutions) (BD Bioscience). For intracellular staining, antibodies against TNF (MP6-XT22; 1:200 dilutions) and IFN-γ (XMG1.2; 1:200 dilutions) were used in combination with anti-CD4 and anti-CD8 antibodies. To detect intracellular cytokines in T cells from the lungs, single cell suspensions (1.0×10^6 cells) were stimulated following peptides or PPD respectively at 37 °C for 6 h in the presence of both GolgiPlug and GolgiStop (BD Biosciences). PPD was kindly provided by Dr. Michael Brennan at Aeras (Rockville, MD, USA). Recombinant Ag85B protein was purchased from Abcam (Waltham, MA, USA). All peptides were synthesized from GenScript (Piscataway, NJ, USA): A mixture of ESAT-6 peptides (1 μg/ml of each peptide) were consisted of 14 peptides (17- and 18-mer peptides) spanning the mature forms of Mtb ESAT-6 and $Ag85B_{240\text{-}254}$ peptide (FQDAYNAAGGHNAVF; 1 μg/ml).

Enumeration of CFU in the Ly6G$^+$ cells

Ly6G$^+$ cells were isolated as previously described from the lungs of each subset of mice using a Myeloid-Derived Suppressor Cell Isolation Kit (Miltenyi Biotec; cat#130-094-538) at 3- and 4-weeks post Mtb infection[35]. Isolated Ly6G$^+$ cells from Mtb infected mice followed by Gem treatment and Mtb infected only mice were lysed with 0,05% Triton X-100 (Biosesang, Gyeonggi-go, Republic of Korea), and the lysates were plated onto 7H10-OADC agar to enumerate the bacteria.

Antibody-mediated in vivo blockade

Neutrophil depletion: 250 μg of anti-Ly6G (1A8; Bio X cell, Lebanon, NH, USA) or rat IgG2a isotype control (2A3; Bio X cell) were administered to Mtb-infected mice at 14, 16, 18 days post Mtb infection via intraperitoneal route. G-CSF neutralization: 50 μg of anti-G-CSF antibody (67604; R&D systems) or rat IgG1 isotype control (43414; R&D systems) were administered to mice starting at 13 days post infection, every alternate day till day 27 via intraperitoneal route. IFN-γ neutralization: 250 μg of anti-IFN-γ (XMG1.2; Bio X cell) or rat IgG1 isotype control (HRPN; Bio X cell) were administered to Mtb-infected mice starting at 6 days post infection, every alternate day till day 16. via intraperitoneal route.

Immunofluorescence staining

For confirming Ly6G$^+$ cell depletion, lung tissue sections (4-5 μm) were cut from formalin-fixed paraffin-embedded (FFPE) blocks were dewaxed and re-hydrated before staining. Antigen retrieval was performed using pH 8.0 citrate buffer in a microwave. Samples were blocked with 1% BSA in PBS for 1 h at RT, then incubated overnight with rat anti-mouse 1A8 (Biolegend) at 4 °C. After washing samples with PBS, sections were incubated with secondary donkey anti-rat IgG antibody conjugated with Alexa Fluor 594 (Thermo Fisher) for 1 h at RT. Slides were mounted with Vectashield Mounting Medium with DAPI (Vector Laboratories, Newark, CA, USA). Images were acquired using an Olympus IX73 microscope with CellSens Standard software and analysis performed with ImageJ.

Quantification of cytokines

Supernatants of homogenized lung lysates were analyzed for detecting cytokines according to the manufacturer's instructions. The levels of IL-1β, TNF, MCP-1, IL-6, and IL-17A were measured using a LEGENDplex Multi-Analyte Flow Assay Kit (Biolegend; cat#740446). The IL-10 concentration was measured using an ELISA kit from ThermoFisher Scientific (cat#88-7105-88), and the IFN-γ concentration was determined using an ELISA kit from Biolegend (cat#430804). The G-CSF concentration in the serum was analyzed using a Mouse G-CSF Quantikine ELISA kit (R&D Systems, Minneapolis, MN, USA; cat#MCS00).

T cell suppression assay

Ly6G$^+$ cells were isolated as previously described[35]. CD4$^+$ T cells were then isolated from the spleens of C57BL/6J wild-type mice using a CD4$^+$ T cell isolation kit (Miltenyi Biotec; cat#130-104-454) and labeled with a CellTrace Violet Cell Proliferation kit (Thermo Fisher Scientific; cat#C34557). After labeling, CD4$^+$ T cells were stimulated with anti-CD3/28 (2 μg/ml each; Clone 145-2C11/37.51, BD Bioscience) and co-cultured with varying ratios of Ly6G$^+$ cells. After 72 h of co-culture, the cells were harvested, stained, and analyzed by flow cytometry. As an independent experiment, mice were injected TC-1 cancer cell line (5.0×10^5 cells/mouse) via intravenous route and Ly6G$^+$ cells were isolated from the lungs at 17 days post injection. After 72 h of co-culture with labeled CD4$^+$ T cells, proliferation was measured by flow cytometry. Mice were monitored daily for health and weighted twice weekly throughout the study. No mice experienced a weight loss exceeding 20% of their initial body weight.

Adoptive cell transfer

For CD4$^+$ T cell enrichment, CD4$^+$ T cells were isolated from the spleen of wild-type P25 mice by a MagniSort Mouse CD4 T$^+$ T Cell Enrichment Kit (Thermo Fisher; cat#8804-6821-74). For adoptive transfer of P25 CD4$^+$ T cells, the cells were isolated from the spleen of naïve P25 mice after CD4$^+$ T cell enrichment. After isolation, 2×10^6 purified Thy1.1$^+$CD4$^+$ or Ly5.1$^+$CD4$^+$ T cells were transferred into wild-type C57BL/6 mice via the tail vein. Mice were infected with Mtb 1 day after adoptive transfer.

BCG immunization

BCG was administered subcutaneously at a dose of 1.0×10^6 CFUs, 8 weeks prior to Mtb infection.

Statistics

Data for all experiments are presented as the mean ± standard deviation (SD). For analysis of cells from patients, Wilcoxon matched pairs test was used to compare baseline and after treatment. For immunological analysis, the significance of differences between samples was assessed by one-way or two-way ANOVA after Tukey's post test for multiple comparisons in more than three groups or by unpaired *t*-test in the selected two groups. For CFU and histopathology analysis, the Mann-Whitney rank test was used when comparing the differences between two different groups. Kaplan–Meier survival curves were analyzed using the Mantel–Cox log-rank test with a 95% CI. For statistical analysis, GraphPad Prism version 8.00 for Windows was used (GraphPad Software, La Jolla California USA, www.graphpad.com). Differences with each value of $^*p < 0.05$, $^{**}p < 0.01$, $^{***}p < 0.001$, or $^{****}p < 0.0001$ were considered statistically significant. The figures and figure legends include detailed statistical information such as the type of statistical test used, the exact sample size (*n*), the precision measures, and the threshold for statistical significance.

Reporting summary

Further information on research design is available in the Nature Portfolio Reporting Summary linked to this article.

Data availability

The main data generated in this study supporting the findings are available within the article and the main data are provided in the Supplementary Information and Source Data files or from the corresponding author on request. Source data are provided with this paper.

References

1. Bagcchi, S. WHO's global tuberculosis report 2022. *Lancet Microbe* **4**, e20 (2023).
2. Kwon, K. W. et al. BCG-booster vaccination with HSP90-ESAT-6-HspX-RipA multivalent subunit vaccine confers durable protection against hypervirulent Mtb in mice. *NPJ Vaccines* **9**, 55 (2024).
3. Zak, D. E. et al. A blood RNA signature for tuberculosis disease risk: a prospective cohort study. *Lancet* **387**, 2312–2322 (2016).
4. Barry, C. E. et al. The spectrum of latent tuberculosis: rethinking the biology and intervention strategies. *Nat. Rev. Microbiol.* **7**, 845–855 (2009).
5. Walzl, G., Ronacher, K., Hanekom, W., Scriba, T. J. & Zumla, A. Immunological biomarkers of tuberculosis. *Nat. Rev. Immunol.* **11**, 343–354 (2011).
6. Dobler, C. C., Cheung, K., Nguyen, J. & Martin, A. Risk of tuberculosis in patients with solid cancers and haematological malignancies: a systematic review and meta-analysis. *Eur. Respir. J.* **50**, 1700157 (2017).
7. Horsburgh, C. R. Jr. Priorities for the treatment of latent tuberculosis infection in the United States. *N. Engl. J. Med.* **350**, 2060–2067 (2004).
8. Cheng, M. P. et al. Risk of active tuberculosis in patients with cancer: a systematic review and meta-analysis. *Clin. Infect. Dis.* **64**, 635–644 (2017).
9. Cohn, D. L. et al. Targeted tuberculin testing and treatment of latent tuberculosis infection. *Morb. Mortal. Wkly. Rep.* **49**, 1–54 (2000).
10. Bae, S. et al. Risk of tuberculosis in patients with cancer treated with immune checkpoint inhibitors: a nationwide observational study. *J. Immunother. Cancer* **9**, e002960 (2021).
11. Simonsen, D. F., Farkas, D. K., Horsburgh, C. R., Thomsen, R. W. & Sørensen, H. T. Increased risk of active tuberculosis after cancer diagnosis. *J. Infect.* **74**, 590–598 (2017).
12. Seo, G. H. et al. Cancer-specific incidence rates of tuberculosis: a 5-year nationwide population-based study in a country with an intermediate tuberculosis burden. *Medicine* **95**, e4919 (2016).
13. Kim, H. R. et al. Solid-organ malignancy as a risk factor for tuberculosis. *Respirology* **13**, 413–419 (2008).
14. La Manna, M. P. et al. Quantitative and qualitative profiles of circulating monocytes may help identifying tuberculosis infection and disease stages. *PLoS ONE* **12**, e0171358 (2017).
15. Wang, W. et al. Value of the ratio of monocytes to lymphocytes for monitoring tuberculosis therapy. *Can. J. Infect. Dis. Med. Microbiol.* **2019**, 3270393 (2019).
16. Rakotosamimanana, N. et al. Biomarkers for risk of developing active tuberculosis in contacts of TB patients: a prospective cohort study. *Eur. Respir. J.* **46**, 1095–1103 (2015).
17. Jeon, Y., Lee, W. I., Kang, S. Y. & Kim, M. H. Neutrophil-to-monocyte-plus-lymphocyte ratio as a potential marker for discriminating pulmonary tuberculosis from nontuberculosis infectious lung diseases. *Lab Med.* **50**, 286–291 (2019).
18. Miyahara, R. et al. Predicting the risk of pulmonary tuberculosis based on the neutrophil-to-lymphocyte ratio at TB screening in HIV-infected individuals. *BMC Infect. Dis.* **19**, 667 (2019).
19. Naranbhai, V. et al. Ratio of monocytes to lymphocytes in peripheral blood identifies adults at risk of incident tuberculosis among HIV-infected adults initiating antiretroviral therapy. *J. Infect. Dis.* **209**, 500–509 (2014).
20. Naranbhai, V. et al. The association between the ratio of monocytes:lymphocytes at age 3 months and risk of tuberculosis (TB) in the first two years of life. *BMC Med.* **12**, 120 (2014).
21. Kissling, M. et al. Monocyte, lymphocyte and neutrophil ratios—easy-to-use biomarkers for the diagnosis of pediatric tuberculosis. *Pediatr. Infect. Dis. J.* **42**, 520–527 (2023).
22. Gideon, H. P., Skinner, J. A., Baldwin, N., Flynn, J. L. & Lin, P. L. Early whole blood transcriptional signatures are associated with severity of lung inflammation in cynomolgus macaques with *Mycobacterium tuberculosis* infection. *J. Immunol.* **197**, 4817–4828 (2016).
23. Scriba, T. J. et al. Sequential inflammatory processes define human progression from *M. tuberculosis* infection to tuberculosis disease. *PLoS Pathog.* **13**, e1006687 (2017).
24. Eum, S. Y. et al. Neutrophils are the predominant infected phagocytic cells in the airways of patients with active pulmonary TB. *Chest* **137**, 122–128 (2010).
25. Gopal, R. et al. S100A8/A9 proteins mediate neutrophilic inflammation and lung pathology during tuberculosis. *Am. J. Respir. Crit. Care Med.* **188**, 1137–1146 (2013).
26. Moreira-Teixeira, L. et al. Type I IFN exacerbates disease in tuberculosis-susceptible mice by inducing neutrophil-mediated lung inflammation and NETosis. *Nat. Commun.* **11**, 5566 (2020).
27. Lovewell, R. R., Baer, C. E., Mishra, B. B., Smith, C. M. & Sassetti, C. M. Granulocytes act as a niche for *Mycobacterium tuberculosis* growth. *Mucosal Immunol.* **14**, 229–241 (2021).
28. Berry, M. P. et al. An interferon-inducible neutrophil-driven blood transcriptional signature in human tuberculosis. *Nature* **466**, 973–977 (2010).
29. Mishra, B. B. et al. Nitric oxide prevents a pathogen-permissive granulocytic inflammation during tuberculosis. *Nat. Microbiol.* **2**, 17072 (2017).
30. Nouailles, G. et al. CXCL5-secreting pulmonary epithelial cells drive destructive neutrophilic inflammation in tuberculosis. *J. Clin. Invest.* **124**, 1268–1282 (2014).
31. Kimmey, J. M. et al. Unique role for ATG5 in neutrophil-mediated immunopathology during *M. tuberculosis* infection. *Nature* **528**, 565–569 (2015).
32. Marzo, E. et al. Damaging role of neutrophilic infiltration in a mouse model of progressive tuberculosis. *Tuberculosis* **94**, 55–64 (2014).
33. Niazi, M. K. et al. Lung necrosis and neutrophils reflect common pathways of susceptibility to *Mycobacterium tuberculosis* in genetically diverse, immune-competent mice. *Dis. Model Mech.* **8**, 1141–1153 (2015).
34. Maxwell, M. B. & Maher, K. E. Chemotherapy-induced myelosuppression. *Semin. Oncol. Nurs.* **8**, 113–123 (1992).
35. Kang, T. G. et al. Viral coinfection promotes tuberculosis immunopathogenesis by type I IFN signaling-dependent impediment of Th1 cell pulmonary influx. *Nat. Commun.* **13**, 3155 (2022).
36. Vanickova, K. et al. Hematopoietic stem cells undergo a lymphoid to myeloid switch in early stages of emergency granulopoiesis. *EMBO J.* **42**, e113527 (2023).
37. Boettcher, S. et al. Endothelial cells translate pathogen signals into G-CSF-driven emergency granulopoiesis. *Blood* **124**, 1393–1403 (2014).
38. Manz, M. G. & Boettcher, S. Emergency granulopoiesis. *Nat. Rev. Immunol.* **14**, 302–314 (2014).
39. Knaul, J. K. et al. Lung-residing myeloid-derived suppressors display dual functionality in murine pulmonary tuberculosis. *Am. J. Respir. Crit. Care Med.* **190**, 1053–1066 (2014).
40. Mikyšková, R. et al. Cyclophosphamide-induced myeloid-derived suppressor cell population is immunosuppressive but not identical to myeloid-derived suppressor cells induced by growing TC-1 tumors. *J. Immunother.* **35**, 374–384 (2012).

41. Tamura, T. et al. The role of antigenic peptide in CD4+ T helper phenotype development in a T cell receptor transgenic model. *Int. Immunol.* **16**, 1691–1699 (2004).
42. Delahaye, J. L. et al. Cutting edge: bacillus calmette-guérin-induced T cells shape *Mycobacterium tuberculosis* infection before reducing the bacterial burden. *J. Immunol.* **203**, 807–812 (2019).
43. Buechler, M. B., Teal, T. H., Elkon, K. B. & Hamerman, J. A. Cutting edge: type I IFN drives emergency myelopoiesis and peripheral myeloid expansion during chronic TLR7 signaling. *J. Immunol.* **190**, 886–891 (2013).
44. Gröschel, M. I. et al. Recombinant BCG expressing ESX-1 of *Mycobacterium marinum* combines low virulence with cytosolic immune signaling and improved TB protection. *Cell Rep.* **18**, 2752–2765 (2017).
45. Forget, P. et al. What is the normal value of the neutrophil-to-lymphocyte ratio?. *BMC Res. Notes* **10**, 12 (2017).
46. Prozan, L. et al. Prognostic value of neutrophil-to-lymphocyte ratio in COVID-19 compared with Influenza and respiratory syncytial virus infection. *Sci. Rep.* **11**, 21519 (2021).
47. Lowsby, R. et al. Neutrophil to lymphocyte count ratio as an early indicator of blood stream infection in the emergency department. *Emerg. Med. J.* **32**, 531–534 (2015).
48. de Jager, C. P. et al. The neutrophil-lymphocyte count ratio in patients with community-acquired pneumonia. *PLoS ONE* **7**, e46561 (2012).
49. Yin, Y. et al. Pretreatment neutrophil-to-lymphocyte ratio in peripheral blood was associated with pulmonary tuberculosis retreatment. *Arch. Med. Sci.* **13**, 404–411 (2017).
50. Aldabbagh, M. A. et al. The PREVALEnce of *Mycobacterium tuberculosis* infection among cancer patients receiving chemotherapy in a tertiary care center. *Cureus* **14**, e32068 (2022).
51. Gu, Z. et al. Association of blood neutrophil-lymphocyte ratio with short-term prognosis and severity of tuberculosis meningitis patients without HIV infection. *BMC Infect. Dis.* **23**, 449 (2023).
52. Osmani, A. H., Jabbar, A. A., Gangwani, M. K. & Hassan, B. Outcomes of high risk patients with febrile neutropenia at a tertiary care center. *Asian Pac. J. Cancer Prev.* **18**, 2741–2745 (2017).
53. Hashiguchi, Y. et al. Chemotherapy-induced neutropenia and febrile neutropenia in patients with gynecologic malignancy. *Anticancer Drugs* **26**, 1054–1060 (2015).
54. Shokane, L. L., Bezuidenhout, S. & Lundie, M. Use of granulocyte colony-stimulating factor in patients with chemotherapy-induced neutropaenia. *Health SA* **28**, 2221 (2023).
55. Xiong, H. et al. Distinct contributions of neutrophils and CCR2+ monocytes to pulmonary clearance of different *Klebsiella pneumoniae* strains. *Infect. Immun.* **83**, 3418–3427 (2015).
56. Garvy, B. A. & Harmsen, A. G. The importance of neutrophils in resistance to *pneumococcal pneumonia* in adult and neonatal mice. *Inflammation* **20**, 499–512 (1996).
57. Yang, C. T. et al. Neutrophils exert protection in the early tuberculous granuloma by oxidative killing of mycobacteria phagocytosed from infected macrophages. *Cell Host Microbe* **12**, 301–312 (2012).
58. Dallenga, T. & Schaible, U. E. Neutrophils in tuberculosis-first line of defence or booster of disease and targets for host-directed therapy? *Pathog. Dis.* **74**, ftw012 (2016).
59. Liu, Q. et al. Proteomic profiling for plasma biomarkers of tuberculosis progression. *Mol. Med. Rep.* **18**, 1551–1559 (2018).
60. Sakai, S. et al. Cutting edge: control of *Mycobacterium tuberculosis* infection by a subset of lung parenchyma-homing CD4 T cells. *J. Immunol.* **192**, 2965–2969 (2014).
61. Wolf, A. J. et al. Initiation of the adaptive immune response to *Mycobacterium tuberculosis* depends on antigen production in the local lymph node, not the lungs. *J. Exp. Med.* **205**, 105–115 (2008).
62. Nandi, B. & Behar, S. M. Regulation of neutrophils by interferon-γ limits lung inflammation during tuberculosis infection. *J. Exp. Med.* **208**, 2251–2262 (2011).
63. Bronte, V., Serafini, P., Mazzoni, A., Segal, D. M. & Zanovello, P. L-arginine metabolism in myeloid cells controls T-lymphocyte functions. *Trends Immunol.* **24**, 302–306 (2003).
64. Serafini, P. Myeloid derived suppressor cells in physiological and pathological conditions: the good, the bad, and the ugly. *Immunol. Res.* **57**, 172–184 (2013).
65. Orme, I. M., Robinson, R. T. & Cooper, A. M. The balance between protective and pathogenic immune responses in the TB-infected lung. *Nat. Immunol.* **16**, 57–63 (2015).
66. de Bruin, A. M. et al. IFNγ induces monopoiesis and inhibits neutrophil development during inflammation. *Blood* **119**, 1543–1554 (2012).
67. Murray, P. J., Young, R. A. & Daley, G. Q. Hematopoietic remodeling in interferon-gamma-deficient mice infected with mycobacteria. *Blood* **91**, 2914–2924 (1998).
68. Pearl, J. E., Saunders, B., Ehlers, S., Orme, I. M. & Cooper, A. M. Inflammation and lymphocyte activation during mycobacterial infection in the interferon-gamma-deficient mouse. *Cell Immunol.* **211**, 43–50 (2001).
69. Norose, K., Naoi, K., Fang, H. & Yano, A. In vivo study of toxoplasmic parasitemia using interferon-gamma-deficient mice: absolute cell number of leukocytes, parasite load and cell susceptibility. *Parasitol. Int.* **57**, 447–453 (2008).
70. MacNamara, K. C. et al. Infection-induced myelopoiesis during intracellular bacterial infection is critically dependent upon IFN-γ signaling. *J. Immunol.* **186**, 1032–1043 (2011).
71. Franzke, A. et al. G-CSF as immune regulator in T cells expressing the G-CSF receptor: implications for transplantation and autoimmune diseases. *Blood* **102**, 734–739 (2003).
72. Ray, A. L. et al. G-CSF is a novel mediator of T-cell suppression and an immunotherapeutic target for women with colon cancer. *Clin. Cancer Res.* **29**, 2158–2169 (2023).
73. MacDonald, K. P. et al. Modification of T cell responses by stem cell mobilization requires direct signaling of the T cell by G-CSF and IL-10. *J. Immunol.* **192**, 3180–3189 (2014).
74. Park, S. I., Soki, F. N. & McCauley, L. K. Roles of bone marrow cells in skeletal metastases: no longer bystanders. *Cancer Microenviron.* **4**, 237–246 (2011).
75. Shiozawa, Y. et al. Human prostate cancer metastases target the hematopoietic stem cell niche to establish footholds in mouse bone marrow. *J. Clin. Invest.* **121**, 1298–1312 (2011).
76. Messmer, M. N., Netherby, C. S., Banik, D. & Abrams, S. I. Tumor-induced myeloid dysfunction and its implications for cancer immunotherapy. *Cancer Immunol. Immunother.* **64**, 1–13 (2015).
77. Alvarez, R., Oliver, L., Valdes, A. & Mesa, C. Cancer-induced systemic myeloid dysfunction: implications for treatment and a novel nanoparticle approach for its correction. *Semin. Oncol.* **45**, 84–94 (2018).
78. Gabrilovich, D. Mechanisms and functional significance of tumour-induced dendritic-cell defects. *Nat. Rev. Immunol.* **4**, 941–952 (2004).
79. Rolston, K. V. Infections in cancer patients with solid tumors: a review. *Infect. Dis. Ther.* **6**, 69–83 (2017).
80. Kim, D. K. et al. Clinical characteristics and treatment responses of tuberculosis in patients with malignancy receiving anticancer chemotherapy. *Chest* **128**, 2218–2222 (2005).
81. Plumlee, C. R. et al. Ultra-low dose aerosol infection of mice with *Mycobacterium tuberculosis* more closely models human tuberculosis. *Cell Host Microbe* **29**, 68–82.e65 (2021).
82. Lerner, T. R. et al. *Mycobacterium tuberculosis* replicates within necrotic human macrophages. *J. Cell Biol.* **216**, 583–594 (2017).
83. Kaufmann, E. et al. BCG educates hematopoietic stem cells to generate protective innate immunity against tuberculosis. *Cell* **172**, 176–190.e119 (2018).

84. Tran, K. A. et al. BCG immunization induces CX3CR1(hi) effector memory T cells to provide cross-protection via IFN-γ-mediated trained immunity. *Nat. Immunol.* **25**, 418–431 (2024).

Acknowledgements

We acknowledge the NIH Tetramer Core Facility for provision of I-A(b):ESAT-6_{4-17}, I-A(b):Ag85$B_{280-294}$-and corresponding negative control tetramers I-A(b):hCLIP. This work was supported by the National Research Foundation of Korea (NRF) grant funded by the Korea government (MSIT) (RS-2024-00392705 to S.-J.H.; RS-2023-00208115 to S.J.S.; RS-2023-00210371, RS-2022-00164735 to K.W.K.), Republic of Korea. The funders had no role in study design, data collection and analysis, decision to publish, or preparation of the manuscript. The work was supported in part by Brain Korea 21 (BK21) FOUR program. M.C.P. is fellowship awardee by the BK21 FOUR program.

Author contributions

Conceptualization: S.J.S. and S.-J.H.; Funding acquisition: K.W.K., S.J.S. and S.-J.H.; Investigation: K.W.K., T.G.K., E.C., H.K., M.C.P., S.C., K.K., and H.W.K.; Methodology: K.W.K., T.G.K., E.C., H.K., M.C.P., S.C., K.K., and H.W.K.; Patients management: J.B.L., S.J.J., and H.R.K.; Supervision: S.J.S. and S.-J.H.; Validation: S.J.S. and S.-J.H.; Writing—original draft: K.W.K., T.G.K., S.J.S., and S.-J.H.; Writing—review and editing: K.W.K., T.G.K., S.J.S., and S.-J.H. with inputs from all authors.

Competing interests

The authors declare no competing interests.

Additional information

Supplementary information The online version contains supplementary material available at https://doi.org/10.1038/s41467-025-63930-0.

Correspondence and requests for materials should be addressed to Sung Jae Shin or Sang-Jun Ha.

Peer review information *Nature Communications* thanks Amit Singhal, who co-reviewed with Sakshi Agarwal and the other, anonymous, reviewer(s) for their contribution to the peer review of this work. A peer review file is available.